

UC San Diego

UC San Diego Electronic Theses and Dissertations

Title

Genetically encoded optical control of protein function

Permalink

<https://escholarship.org/uc/item/4qd6f1rw>

Author

Meijer, René Marcel

Publication Date

2006

Peer reviewed|Thesis/dissertation

UNIVERSITY OF CALIFORNIA, SAN DIEGO

**Genetically Encoded Optical Control of Protein
Function**

A dissertation submitted in partial satisfaction of the
requirements for the degree
Doctor of Philosophy
in
Biology

by

René Marcel Meijer

Committee in charge:

Professor Roger Tsien, Chair
Professor Edward Callaway
Professor Elizabeth Komives
Professor Satchin Panda
Professor Robert Schmidt
Professor Charles Zuker

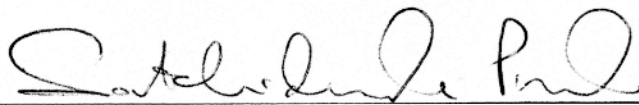
2006

Copyright

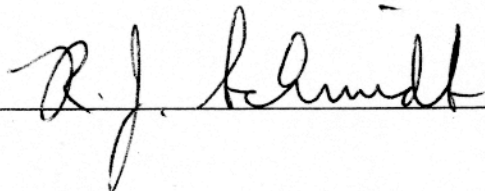
René Marcel Meijer, 2006

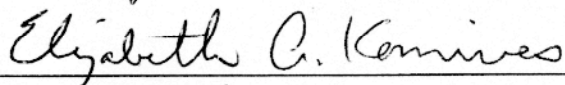
All rights reserved

The dissertation of René Marcel Meijer is approved and it is acceptable in
quality and form for publication on microfilm

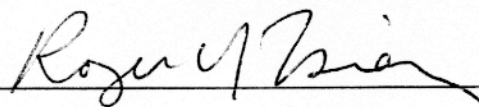












Chair

University of California, San Diego

2006

Table of Contents

Signature Page.....	iii
Table of Contents.....	iv
List of Figures	v
Vita.....	vi
Abstract.....	vii
Chapter 1: An Introduction to Genetically Encoded Control of Protein Function	
Introduction.....	1
References.....	11
Chapter 2: A Retinal Binding Algae Protein Demonstrates No Photocurrents	
Introduction.....	15
Results and Discussion.....	17
Materials and Methods.....	19
Conclusions.....	22
References.....	27
Chapter 3: Heterologous Expression of Functional Light activated Algae Channels	
Introduction.....	30
Results and Discussion.....	33
Materials and Methods.....	39
Conclusions.....	46
References.....	55
Chapter 4: Tetracysteine Motifs on GFP as a Composite Tag	
Introduction.....	57
Results and Discussion.....	64
Materials and Methods.....	76
Conclusions.....	83
References.....	97
Chapter 5: Genetically Encoded Control of Protein Function Conclusion	
Conclusions.....	100
References.....	107

List of Figures

Figure 2.1	Sequence Alignment of COP1, VOP1 and Bacteriorhodopsin	23
Figure 2.2	COP1 and VOP cloned constructs	24
Figure 2.3	COP1 photo-current response	25
Figure 2.4	Immunolabeling of Rho-COP1 construct expression	26
Figure 3.1	ChOP1 and Chop2 channel secondary structure	49
Figure 3.2	ChOP1 and ChOP2 cloned constructs	49
Figure 3.3	Rho-ChOP1-GFP heterologous expression in HEK293 cells	50
Figure 3.4	ChOP1 with fused FLAG epitope and ER export tags	50
Figure 3.5	Rho-ChOP1 construct expression of membrane expression	51
Figure 3.6	ChOP1 construct orientation of membrane expression	52
Figure 3.7	ChOP2 channel secondary structure and response	53
Figure 3.8	ChOP2 channel neuronal response	54
Figure 4.1	FIAsH and ReAsH small molecules and binding configuration	88
Figure 4.2	GFP-TC configuration and ReAsH quantum yields	89
Figure 4.3	Tandem TC constructs and ReAsH quantum yields	90
Figure 4.4	TC GFP insertion quantum yields	91
Figure 4.5	Membrane association of TC tagged GFP constructs	92
Figure 4.6	Multiple TC tagged GFP quantum yields	93
Figure 4.7	Singlet oxygen vs fluorescent quantum yield	94
Figure 4.8	Relative Fluorescence of Cx43-GFP173	95
Figure 4.9	Tomography of Cx43-GFP173	96

Vita

- | | |
|------|--|
| 1986 | B.S., Electrical Engineering, University of Massachusetts, Lowell, Massachusetts |
| 1989 | M.S., Electrical engineering, Tufts University, Medford, Massachusetts |
| 2006 | Ph.D., Biology, University of California, San Diego |

Publications

Tour, O., Meijer, R. M., Zacharias, D. A., Adams, S. R. & Tsien, R. Y.
Genetically targeted chromophore-assisted light inactivation. *Nat. Biotechnol.*
21, 1505-1508 (2003).

ABSTRACT OF THE DISSERTATION

Genetically Encoded Optical Control of Protein Function

by

René Marcel Meijer

Doctor of Philosophy in Biology

University of California, San Diego, 2006

Professor Roger Tsien, Chair

The green alga *Chlamydomonas reinhardtii* has a phototaxis response time less than 50usec, suggesting that the photoreceptor and channel form a protein complex or are a single protein. I extracted and cloned two genes described as opsin type proteins from *C. reinhardtii* algae. When heterologously expressed functional channels in HEK293 cells as well as neurons, one of these channels conducted inward currents upon 477nm illumination.

Photogeneration of singlet oxygen is a viable mechanism for electron-microscopic localization and acute inactivation of biarsenical-tagged proteins. Attachment of multiple fluorophores to a single protein would increase sensitivity if proximity-induced quenching could be avoided. I found that a GFP, used as a rigid scaffold molecule, could be decorated with two tetracysteine motifs, inserted so that the tetracysteines were not palmitoylated,

the GFP retained both free termini, and the bound ReAsH fluorophores maintained full fluorescence and singlet oxygen generation.

Chapter 1

An Introduction to Genetically Encoded Control of Protein Function

Introduction

The brain is comprised of various types of neurons with distinct molecular network organizations. Neural network computation depends on feedback control and the interaction of temporally diverse spiking patterns of different types of neurons that express unique genetic markers and demonstrate heterogeneous wiring properties within neural networks. The functional roles of neurons in information processing have been brought to light by investigating the cause and effect relationship between the neuronal artificial stimulation and the corresponding response.

The direct electrical stimulation and recording of neurons in intact brain tissue have provided many insights into the function of circuit systems. Neurons belonging to a specific class are often sparsely embedded within tissue, posing fundamental challenges for resolving the role of particular neuron types in information processing. The conventional electrical stimulation of the nerve tissue involves mechanical placement of electrodes in the extracellular space. Using this methodology it is easy to control the temporal pattern of activation though in most cases, many neurons in the electrical field are stimulated simultaneously. It is difficult to stimulate a specifically identified class of neuron by its morphology and/or by a molecular marker. This is important for the reconstruction of neural network activity because defined

types of neurons have their specific pattern of activity¹⁻³. Much information can be revealed in the case where a single neuron can be electrically stimulated with an intracellular electrode, unfortunately, the superior spatial and temporal resolutions of single neuron stimulation is usually limited to neurons in culture or slice. The spatial control limitations make it relatively difficult to stimulate in a controlled way, multiple neurons in parallel. One exception is the application of this method in-vivo by the stimulation of a single pyramidal neuron in the motor cortex elucidating the activation stimulus control network of a rat whisker movement⁴.

Optical stimulation methods have raised much attention because of their advantages over conventional electrical stimulation methods. Caged optical probes have sufficient resolutions in space and time, provide parallel stimulations at multiple sites and are convenient and relatively harmless to cells^{5,6}. Substantial advances have been made in the analysis of neuronal connectivity dynamics and geometry through approaches such as the uncaging of glutamate⁷⁻¹⁰ but progress is hindered because uncaging activators is a method that is non cell-type specific and all receptors are activated in the region of activation. Despite these drawbacks, photostimulation of neurons by uncaging glutamate has been successfully applied to identify the sources of functional input to an identified neuron in living brain slices¹¹ and to map glutamate sensitivities on individual Purkinje neurons⁹. Employing infrared wavelength to allow the light to incur less scattering and penetrate further into the tissue would dramatically improve the

current optical probes. The spatial resolution is greatly improved by the use of two-photon uncaging¹². Photostimulation with caged transmitters has some limitations; action potentials are generated in all neuron types near the stimulation site, the firing timing is not tightly controlled and the caged transmitters are applied with difficulty in living animals⁵. The spatio-temporal resolution of classic optical probes for neural coding do not have the capability to resolve single neuronal spikes.

Improved utility of optical control of neuronal membrane potential can be realized when one can introduce an exogenous receptor of the light stimulus by transfection, so that it can be targeted at will to designated subpopulations of neurons or regions of the membrane. Selectivity for particular neurons could result either from specific promoters active in those cells or by using a “gene gun” or viruses to deliver the cDNA in a delimited region remote from the site of eventual illumination. Only those cells with bodies at the site of cDNA delivery and processes extending through the illumination zone would be affected. Furthermore, previous genetically encoded optical methods, although elegant¹³⁻¹⁶, have allowed control of neuronal activity over timescales of seconds to minutes owing to their mechanisms for effecting depolarization. Kinetics roughly a thousand times faster would be necessary to remotely control individual spikes or synaptic events.

We consider here a novel approach to endow photosensitivity to neurons by genetic engineering a photosensitive algal cation channel ectopically expressed in mammalian cells. This is ideal for stimulating a single

neuron or a selected subset of neurons because restricted gene expression is possible with cell-type-specific promoters . This method is also advantageous in that no requirement of the delivery of caged transmitters is necessary^{5,6}. This high temporal resolution, noninvasive, genetically based method to control neural activity could enable elucidation of the temporal activity patterns in specific neurons that drive circuit dynamics, plasticity and behavior.

Photoreception in animals evolved differently in vertebrates and invertebrates although both use a seven-transmembrane (7-TM) helix protein with a covalently linked retinal chromophore as a primary photoreceptor. Rhodopsin initiates a G protein-coupled enzyme cascade in vertebrates that ends in the hydrolysis of cGMP and the closure of the cGMP-regulated cation channels in effect hyperpolarizing the plasma membrane¹⁷⁻¹⁹. Invertebrate rhodopsin also initiates a G protein-coupled signaling cascade, which, however, results in activation of transient receptor potential (TRP) and TRP-like (TRPL) channels and a the subsequent depolarization of the membrane potential^{20,21}. Microbial-type rhodopsins are also 7-TM retinal proteins but show no sequence homology to animal rhodopsins. Bacteriorhodopsin (BR) is the proto-type microbial-type rhodopsin that functions as a light-driven proton pump²². Bacteriorhodopsin is a structurally and functionally well understood model system for active transmembrane ion transport^{23,24} and is the first membrane protein to use macromolecular x-ray crystallography to decipher the structure of the protein. Other microbial rhodopsins include light-driven chloride pumps or light sensors, the latter enabling phototaxis by coupling to

specific transducers²⁵⁻²⁷.

Recently, microbial-type rhodopsins were also found in fungi²⁸ and alga and it has been known since 1991 that phototaxis and photophobic responses in the green alga *Chlamydomonas reinhardtii* are mediated by rhodopsins with a microbial-type *all-trans retinal* chromophore²⁹⁻³¹. As shown for the green algae *Haematococcus pluvialis*³², *C. reinhardtii*, and *Volvox carteri*³³, the photoreceptor currents are confined to the pigmented eyespot region. Although the ion dependence of the photoreceptor currents in these algae is different, it has been proposed for all three species on the basis of stimulus-response curves that they comprise a high-intensity and a low-intensity photoreceptor system with one or more rhodopsin species³³⁻³⁵. For *C. reinhardtii* it was shown that at high flash energies the delay between the flash and the beginning of the photocurrent is <50 μ s, which led to the suggestion that the photoreceptor and the channel form a protein complex³⁶ or are even one and the same protein³⁵. At low flash intensities the photoreceptor current is delayed by several milliseconds, suggesting that the low-intensity photoreceptor system involves a signal amplification system that activates the conductance indirectly³³. Under physiological conditions photoreceptor currents are carried mainly by Ca^{2+} , but K^{+} is also conducted when the driving force is enhanced at high extracellular K^{+} ³⁷. When the eyespot region is exposed to low pH a second proton photoreceptor current component appears³⁵.

Two rhodopsins in the unicellular green alga *Chlamydomonas reinhardtii* were recently identified³⁸. Channel-rhodopsin 1, ChR1 (ChR1=ChOP1 apoprotein + retinal chromophore) is a light-gated proton channel, whereas the other, channel-rhododopsin2, ChR2 (ChR2=ChOP2 apoprotein + retinal chromophore) is a light-gated cation channel. The N-terminal secondary structures of ChOP1 and ChOP2 are homologous to the seven-transmembrane structure of many microbial-type rhodopsins; they compose a channel with light-gated conductance. ChOP2 photo-channels combine some of the best possible features of previous photostimulation methods, including the speed of a monolithic ion channel¹⁴, and the efficacy of light-transduction¹⁶.

In an electrical cell population assay that monitors the differential response of cells facing the light versus cells facing away from the light, the authors demonstrated that both ChR1 and ChR2 contribute to the photoreceptor currents³⁸. Because in ChR1-deprived cells photocurrents at high flash intensities were reduced, whereas in ChR2-deprived cells photocurrents at low flash energies were reduced, the authors concluded that ChR1 mediates the high-intensity response, whereas ChR2 is responsible for low-intensity photocurrents³⁸. The mechanism for how ChR1 and ChR2 contribute to the photocurrents and to what extent to phobic responses and phototaxis could not be resolved. Generation of photocurrent attributed to ChR2 was described as slow and, in analogy to phototaxis in archaea, coupling of a ChR to its specific transducer was proposed, although the

possibility that ChR1 might be an ion channel by itself was taken into account³⁸. It has been shown that expression of ChOP1 in oocytes of *Xenopus laevis* produces a light-gated conductance that is highly selective for protons, and it was demonstrated by generated transformants in which the ratio of ChOP1 and its homolog ChOP2 were changed by an antisense approach, that ChR1 is the photoreceptor system that mediates the proton photoreceptor current³⁸.

We aimed to express the photochannels, ChOP1 and ChOP2, in mammalian cells in the hope of obtaining a functional rhodopsin that would depolarize mammalian cells and might have application as a remote, noninvasive neuron stimulation methodology.

Genetically Encode Multiple Biarsenical Composite GFP Tag

Networks of interacting protein components drive a complex array of cellular processes, many of which cannot be observed when the biomolecules are examined in their purified forms. To study biological processes in the context of living cells requires the ability to track molecules within living cells. Few biomolecules are naturally endowed with features that permit their direct detection. Several methods have been developed to equip cellular components with reporter tags for visualization and isolation from biological samples.

The most popular tagging strategy for cellular imaging involves recombinant fusion of green fluorescent protein (GFP), or related color variants^{39,40}, to the protein of interest. The genetically encoded fusion of these fluorescent probes to a target protein require no auxiliary cofactors other than

O², because the chromophore is generated by spontaneous cyclization and oxidation of three amino acids. GFP tags can be used to analyze protein expression and localization in living cells by visualization and quantification with fluorescence microscopy.

Fluorescent protein fusion reporters are limiting in that they are relatively large proteins and can be a significant steric hindrance and may therefore influence the expression, localization or function of the protein to which they are attached. Small molecule reporters, simply due their small size, are less invasive. Imaging with small molecules requires a means to selectively target the small probe to a desired protein. Nucleophilic functionality occurs in most types of biopolymers, permitting facile derivatization with biotin, fluorophores and numerous other small-molecule reporters. Conjugation of small molecule reporters to their purified target protein in-vitro is trivial but within a living cell remains a formidable challenge.

Combining genetically encoded tags with the specificity of antibody labeling and the versatility of small-molecule probes is a standard method of Immunolabeling a target protein of interest in a cell. Another system uses a recombinant protein modified to include a short peptide sequence containing a tetracysteine motif (CCPGCC) that reacts selectively with biarsenicals^{41,42}. Target protein specificity is ensured by the rarity of the hexapeptide motif among endogenous proteins. The hexapeptide chemical reporter fused to target proteins at the genetic level and is covalently labeled in living cells with membrane-permeant biarsenical dyes, such as the fluorescein derivative

FIAsH and the resorufin derivative ReAsH. The biarsenical probes are only weakly fluorescent when free in solution and undergo a marked increase in fluorescence when bound to the target sequence. Ethanedithiol (EDT) prevents the non-specific labeling of biomolecules bearing isolated cysteine residues. In several studies, FIAsH and ReAsH were used as a photosensitizer, generating singlet oxygen to selectively inactivate proteins to which it is fused (CALI or FALI)^{43,44} or to produce contrast stains for electron microscopy⁴⁵. Because GFP cannot photoconvert, the tetracysteine-biarsenical system offers a unique application of a genetically targetable label that can be viewed by optical microscopy while cells are still alive, then by electron microscopy at much higher resolution.

Chromophore Assisted Laser Inactivation

Gene knockouts, antisense and RNA interference are approaches used to eliminate specific proteins or protein function in-vivo that intrinsically have limited temporal and spatial resolution. A general approach for inactivating specific proteins with high spatial and temporal precision is CALI (chromophore-assisted light inactivation)^{46,46}; Strong illumination of the chromophore generates short-lived singlet oxygen, a reactive oxygen species (ROS), that can inactivate nearly any protein in the immediate vicinity of the chromophore. FIAsH is an efficient photosensitizer and has a reported inactivation range of 3-4 nm^{46,47} though recent experiments have indicated the singlet oxygen impact range is more on the order of 70nm (Colette Dooley, personal communication) . ReAsH offers a balance between efficient

generation of reactive oxygen species and resistance to photobleaching.

References

1. Hutcheon, B. & Yarom, Y. Resonance, oscillation and the intrinsic frequency preferences of neurons. *Trends Neurosci.* **23**, 216-222 (2000).
2. Pike, F. G. et al. Distinct frequency preferences of different types of rat hippocampal neurones in response to oscillatory input currents. *J. Physiol.* **529 Pt 1**, 205-213 (2000).
3. Somogyi, P. & Klausberger, T. Defined types of cortical interneurone structure space and spike timing in the hippocampus. *J. Physiol.* **562**, 9-26 (2005).
4. Brecht, M., Schneider, M., Sakmann, B. & Margrie, T. W. Whisker movements evoked by stimulation of single pyramidal cells in rat motor cortex. *Nature* **427**, 704-710 (2004).
5. Callaway, E. M. & Yuste, R. Stimulating neurons with light. *Curr. Opin. Neurobiol.* **12**, 587-592 (2002).
6. Miesenbock, G. Genetic methods for illuminating the function of neural circuits. *Curr. Opin. Neurobiol.* **14**, 395-402 (2004).
7. Dalva, M. B. & Katz, L. C. Rearrangements of synaptic connections in visual cortex revealed by laser photostimulation. *Science* **265**, 255-258 (1994).
8. Dantzker, J. L. & Callaway, E. M. Laminar sources of synaptic input to cortical inhibitory interneurons and pyramidal neurons. *Nat Neurosci* **3**, 701-707 (2000).
9. Pettit, D. L., Helms, M. C., Lee, P., Augustine, G. J. & Hall, W. C. Local excitatory circuits in the intermediate gray layer of the superior colliculus. *J. Neurophysiol.* **81**, 1424-1427 (1999).
10. Shepherd, G. M., Pologruto, T. A. & Svoboda, K. Circuit analysis of experience-dependent plasticity in the developing rat barrel cortex. *Neuron* **38**, 277-289 (2003).
11. Brivanlou, I. H., Dantzker, J. L., Stevens, C. F. & Callaway, E. M. Topographic specificity of functional connections from hippocampal CA3 to CA1. *Proc Natl Acad Sci U S A* **101**, 2560-2565 (2004).

12. Matsuzaki, M. et al. Dendritic spine geometry is critical for AMPA receptor expression in hippocampal CA1 pyramidal neurons. *Nat Neurosci* **4**, 1086-1092 (2001).
13. Lima, S. Q. & Miesenbock, G. Remote control of behavior through genetically targeted photostimulation of neurons. *Cell* **121**, 141-152 (2005).
14. Banghart, M., Borges, K., Isacoff, E., Trauner, D. & Kramer, R. H. Light-activated ion channels for remote control of neuronal firing. *Nat Neurosci* **7**, 1381-1386 (2004).
15. Zemelman, B. V., Nesnas, N., Lee, G. A. & Miesenbock, G. Photochemical gating of heterologous ion channels: remote control over genetically designated populations of neurons. *Proc Natl Acad Sci U S A* **100**, 1352-1357 (2003).
16. Zemelman, B. V., Lee, G. A., Ng, M. & Miesenbock, G. Selective photostimulation of genetically chARGed neurons. *Neuron* **33**, 15-22 (2002).
17. Kaupp, U. B. Family of cyclic nucleotide gated ion channels. *Curr. Opin. Neurobiol.* **5**, 434-442 (1995).
18. Okada, T., Ernst, O. P., Palczewski, K. & Hofmann, K. P. Activation of rhodopsin: new insights from structural and biochemical studies. *Trends Biochem. Sci.* **26**, 318-324 (2001).
19. Sakmar, T. P., Menon, S. T., Marin, E. P. & Awad, E. S. Rhodopsin: insights from recent structural studies. *Annu Rev Biophys Biomol Struct* **31**, 443-484 (2002).
20. Zuker, C. S. The biology of vision of *Drosophila*. *Proc Natl Acad Sci U S A* **93**, 571-576 (1996).
21. Hardie, R. C. & Raghu, P. Visual transduction in *Drosophila*. *Nature* **413**, 186-193 (2001).
22. Oesterhelt, D. & Stoeckenius, W. Functions of a new photoreceptor membrane. *Proc Natl Acad Sci U S A* **70**, 2853-2857 (1973).
23. Henderson, R. et al. Model for the structure of bacteriorhodopsin based on high-resolution electron cryo-microscopy. *J. Mol. Biol.* **213**, 899-929 (1990).
24. Lanyi, J. K. & Luecke, H. Bacteriorhodopsin. *Curr Opin Struct Biol* **11**, 415-419 (2001).

25. Schmies, G., Engelhard, M., Wood, P. G., Nagel, G. & Bamberg, E. Electrophysiological characterization of specific interactions between bacterial sensory rhodopsins and their transducers. *Proc Natl Acad Sci U S A* **98**, 1555-1559 (2001).
26. Spudich, J. L. & Luecke, H. Sensory rhodopsin II: functional insights from structure. *Curr Opin Struct Biol* **12**, 540-546 (2002).
27. Gordeliy, V. I. et al. Molecular basis of transmembrane signalling by sensory rhodopsin II-transducer complex. *Nature* **419**, 484-487 (2002).
28. Bieszke, J. A. et al. The nop-1 gene of *Neurospora crassa* encodes a seven transmembrane helix retinal-binding protein homologous to archaeal rhodopsins. *Proc Natl Acad Sci U S A* **96**, 8034-8039 (1999).
29. Govorunova, E. G., Sineshchekov, O. A., Gartner, W., Chunaev, A. S. & Hegemann, P. Photoreceptor current and photoorientation in *Chlamydomonas* mediated by 9-demethylchlamarhodopsin. *Biophys. J.* **81**, 2897-2907 (2001).
30. Lawson, M. A., Zacks, D. N., Derguini, F., Nakanishi, K. & Spudich, J. L. Retinal analog restoration of photophobic responses in a blind *Chlamydomonas reinhardtii* mutant. Evidence for an archaeobacterial like chromophore in a eukaryotic rhodopsin. *Biophys. J.* **60**, 1490-1498 (1991).
31. Takahashi, T. et al. Photoisomerization of retinal at 13-ene is important for phototaxis of *Chlamydomonas reinhardtii*: simultaneous measurements of phototactic and photophobic responses. *Biochem. Biophys. Res. Commun.* **178**, 1273-1279 (1991).
32. Litvin, F. F., Sineshchekov, O. A. & Sineshchekov, V. A. Photoreceptor electric potential in the phototaxis of the alga *Haematococcus pluvialis*. *Nature* **271**, 476-478 (1978).
33. Braun, F. J. & Hegemann, P. Two light-activated conductances in the eye of the green alga *Volvox carteri*. *Biophys. J.* **76**, 1668-1678 (1999).
34. Sineshchekov, O. A., Govorunova, E. G., Der, A., Keszthelyi, L. & Nultsch, W. Photoinduced electric currents in carotenoid-deficient *Chlamydomonas* mutants reconstituted with retinal and its analogs. *Biophys. J.* **66**, 2073-2084 (1994).
35. Ehlenbeck, S., Gradmann, D., Braun, F. J. & Hegemann, P. Evidence for a light-induced H(+) conductance in the eye of the green alga *Chlamydomonas reinhardtii*. *Biophys. J.* **82**, 740-751 (2002).

36. Nonnengasser, C., Holland, E. M., Harz, H. & Hegemann, P. The nature of rhodopsin-triggered photocurrents in *Chlamydomonas*. II. Influence of monovalent ions. *Biophys. J.* **70**, 932-938 (1996).
37. Holland, E. M., Braun, F. J., Nonnengasser, C., Harz, H. & Hegemann, P. The nature of rhodopsin-triggered photocurrents in *Chlamydomonas*. I. Kinetics and influence of divalent ions. *Biophys. J.* **70**, 924-931 (1996).
38. Sineshchekov, O. A., Jung, K. H. & Spudich, J. L. Two rhodopsins mediate phototaxis to low- and high-intensity light in *Chlamydomonas reinhardtii*. *Proc Natl Acad Sci U S A* **99**, 8689-8694 (2002).
39. Shaner, N. C., Steinbach, P. A. & Tsien, R. Y. A guide to choosing fluorescent proteins. *Nat Methods* **2**, 905-909 (2005).
40. Lukyanov, K. A., Chudakov, D. M., Lukyanov, S. & Verkhusha, V. V. Innovation: Photoactivatable fluorescent proteins. *Nat Rev Mol Cell Biol* **6**, 885-891 (2005).
41. Griffin, B. A., Adams, S. R., Jones, J. & Tsien, R. Y. Fluorescent labeling of recombinant proteins in living cells with FIAsH. *Methods Enzymol.* **327**, 565-578 (2000).
42. Adams, S. R. et al. New biarsenical ligands and tetracysteine motifs for protein labeling in vitro and in vivo: synthesis and biological applications. *J. Am. Chem. Soc.* **124**, 6063-6076 (2002).
43. Tour, O., Meijer, R. M., Zacharias, D. A., Adams, S. R. & Tsien, R. Y. Genetically targeted chromophore-assisted light inactivation. *Nat. Biotechnol.* **21**, 1505-1508 (2003).
44. Marek, K. W. & Davis, G. W. Transgenically encoded protein photoinactivation (FIAsH-FALI): acute inactivation of synaptotagmin I. *Neuron* **36**, 805-813 (2002).
45. Gaietta, G. et al. Multicolor and electron microscopic imaging of connexin trafficking. *Science* **296**, 503-507 (2002).
46. Beck, S. et al. Fluorophore-assisted light inactivation: a high-throughput tool for direct target validation of proteins. *Proteomics* **2**, 247-255 (2002).
47. Surrey, T. et al. Chromophore-assisted light inactivation and self-organization of microtubules and motors. *Proc Natl Acad Sci U S A* **95**, 4293-4298 (1998).

Chapter 2

A Retinal Binding Algae Protein Demonstrates No Photo-currents

Introduction

There is a significant body of knowledge on optical activation of proteins. Indirect approaches to photoactivate receptor proteins include:

- Uncaging a ligand from an inactive precursor¹
- protein conformational change through a covalently attached synthetic molecule that is directly photoisomerizable^{2,3}
- receptor ligand binding through a photoisomerizable tether⁴.

These approaches have been applied to channels to photostimulate neural activity but each had noteworthy limitations. Caged neurotransmitters have been shown to be an effective method of activating neurons though reversal is limited by the diffusion kinetics of the uncaged ligand⁵. Light induced exogenous expression of ion channels suffers from temporal restrictions due to the relative slow nature of gene activation and repression^{6,7}. Heterologous expression of ion transporter and its ligand improves the temporal control but reversibility is ligand diffusion limited^{8,9}. Exogenous expression of a rhodopsin based signal transduction cascade exhibits a slow light response and neuron dependent onset and offset¹⁰. In contrast, *In-vivo* measurements of the *Chlamydomonas reinhardtii* eye spots indicated that microbial retinal binding opsin proteins (rhodopsins) initiate a subsecond light-gated ion phototaxis response suggesting single photoreceptor-channel protein complex

transporter activity^{11,12}. If heterologous expression of microbial photoreceptor could confer the same light gated ion response in neurons, many of the limitations of the stated approaches could be mitigated.

Retinal Binding Assay

The phototaxis action spectrum of *C. reinhardtii* strongly implicated retinal as the sensor chromophore¹³. Initial reports¹⁴ demonstrated restoration of phototaxis with the application of supplemental retinal in blind retinal-deficient *C. reinhardtii* cells, providing direct convincing evidence that the phototaxis photoreceptor was a rhodopsin. The chromophore was characterized *in-vivo* using supplemented retinal isomers and a behavioral assay. The conclusion was that the algal rhodopsin contained an all-trans retinal chromophore that isomerized upon light exposure to 13-cis retinal in a similar manner as Achaean rhodopsin activation¹⁵⁻¹⁷. To isolate the effector phototaxis protein, retinal was used as the bait for the affinity purification of proteins from the eyespots of *C. reinhardtii*. The most abundant retinal-binding eyespot protein was assumed to be responsible for phototaxis and named Chlamydomonas Opsin Protein 1 (COP1)^{18,19}. Supporting the idea that COP1 (fig 2.1) was the rhodopsin responsible for phototaxis was that a rhodopsin protein, VOP1, of equal molecular weight and high homology to COP1 was retinal affinity purified from *Volvox carteri*, another algae with a rhodopsin phototaxis action spectra.

Chlamydomonas Opsin 1 - COP1

The COP1 sequence was reported as a unique opsin that exhibited no homology to any archaeal opsins. Two possible transmembrane helical domains were speculated to tetramerize to form a channel. There was no sequence reminiscent of other photoactive retinal binding sites. The retinal binding protein was uncharacteristically highly charged and showed no similarities to 7 transmembrane bacteriorhodopsin but some homology to invertebrate opsins and was thought to represent a new class of retinylidene proteins¹⁸. It was proposed from the electrophysiological data that COP1 could form a complex with an ion channel protein to account for the high light ion conductances that were generated for the photophobic response²⁰. The heterologous expression of COP1 in oocytes showed no light gated channel activity²¹. Initial attempts at in-vivo gene silencing produced unstable transformants and were not conclusive.

Results and Discussion

COP1 and VOP1 Constructs

I obtained the genes for COP1 and VOP1 from Dr. Peter Hegemann and cloned them into the mammalian expression vector pCDNA3 (Invitrogen) with a preceding initial N terminal Kozak sequence. To determine if the purported photochannel was readily expressed and integrated into the plasma membrane, the COP1 construct was transiently transfected into HEK293 (ATCC) cells. Whole cell patch clamp exhibited no light gated current

response. In an attempt to ensure heterologous expression on the plasma membrane of the HEK293 cells, I fused the first 39 amino acids of bovine rhodopsin to the N terminus of the COP1 expression construct. This leader sequence has been reported to facilitate translocation of other reporters to the plasma membrane²² (fig 2.2). This Rho-COP1 construct was transiently co-transfected into HEK293 cells with GFP to identify the transfected cells. The fluorescent HEK293 cells were whole cell patchclamped. One cell out of 20 cells tested appeared to exhibit a delayed, noisy photo-response current that depolarized the cell (fig 2.3) but the measurement was not reproducible despite many attempts under various conditions.

Encouraged by the single positive response, we decided we needed to increase any photocurrent response by increasing the Rho-COP1 membrane expression. Expression of the Rho-COP1 fusion should deliver the Rho epitope protruding outside the plasma membrane enabling live cell immunolabeling of Rho. Live cell immunostaining of the protruding Rho tag indicated that there was limited punctate membrane expression (fig 2.4a). I tried adding 2% glycerol to the cell media because it has been reported to be an effective protein chaperone to improve endoplasmic reticulum (ER) export, and increase membrane expression. Added glycerol seemed to improve the plasma membrane targeting but also tended to compromise the health of the cells as was evident from the rounded morphology of the cells (fig 2.4b).

It was not apparent at this time if a fused fluorescent protein would interfere with the function of the channel, but to easily verify specific cell

transfection and degree of membrane expression, CFP was appended to the C terminus of the Rho-COP construct to verify that it was reaching the membrane of the HEK293 cells. Fluorescent cells exhibited a significant amount of fluorescence on the plasma membrane, but there was also significant retention in the ER. Fluorescent cells were whole cell patchclamped but exhibited no light gated current response. In order to equilibrate the degree of expression of each cell and control the loading of the retinal, a stable cell line of the Rho-COP1-CFP construct was created and membrane expression was enhanced by FACS sorting CFP tagged COP1 expressing cells. The cells expressing high levels of Rho-COP1-CFP survived but did not exhibit photocurrents and cell depolarization.

Because we were unable to show light activated responses of COP1 in HEK293 cells, we tried to express the construct directly in neurons. A high cell transfection rate was achieved using a gene gun to shoot gold beads coated with Rho-COP1 and GFP cDNA into mouse brain tissue slices and HEK293 cells. Three transfected neurons and four transfected HEK293 cells were successfully patchclamped with no response with the addition of retinal and light stimulus.

Materials and Methods

Cell Culture

HEK293T (ATCC) cells were cultured in Dulbecco's Modified Eagle's Medium (DMEM) supplemented with 10% fetal bovine serum and 1%

penicillin/streptomycin (enriched DMEM). The cells were grown for 24 hours to approximately 40% confluence, transiently transfected using FuGENE 6 (Roche) and examined 24 hours to 48 hours after transfection. The Cell media was replaced 12 hours post FuGENE transfection with enriched DMEM supplemented with 10uM all trans retinal. Stable HEK293 cells were selected with 1ug/ml G418 (Invitrogen) and maintained with 600ng/ml G418. Cells were grown to 80% confluence and passed 3 times before sorting for GFP fluorescence on Becton Dickinson FACS-Vantage DiVa flow cytometer.

Rho-COP1 Construct

The 117 nucleotide Rho bovine membrane targeting domain sequence was appended to the N terminal of COP1 using primerless PCR. The amino terminus of the Rho fragment was extended with a BamHI site with the primer 5'-ATGAACGGGACCGAGGGCCC-3' and the carboxyl terminus included the initial 12 nucleotides of the COP1 sequence using the primer 5'-TTGAAGTC CATCATGGAGAA-3'. A second PCR product added the distal 12 nucleotides of the Rho tag to the COP1 N terminal and an EcoRI restriction site was added to the C terminal using the primers 5'-TTCTCCATGATGGACTTCAA-3' and 5'-CTACGCTTGTACGAGTGTAG-3'. The two PCR products were verified on an agarose gel. The Rho and COP1 bands of 150bp and 700bp respectively were excised and flash frozen in liquid nitrogen and then spun down at 24000g for 5 minutes to release the DNA from the gel. One μ l from each supernatant sample was added to a PCR reaction as the template using the 5'Rho and 3'COP1 primers. The PCR product was a Rho-COP1 fusion gene

of 850bp which was verified on an agarose gel and gel purified on a gel purification column (Qiagen).

Microscopy and Electrophysiology

Whole-cell patch-clamp recordings were performed by Dr. Oded Tour using ChR2 expressing HEK293 cells visually identified under conventional epifluorescent microscopy (Diaphot microscope, Nikon) equipped with a 40X, 1.3 NA oil objective lens (40x /1.3NA Fluor, Nikon), using a conventional patch clamp system (Axopatch 200A plus Digidata1200, Molecular Devices Co.). The bath solution contained 140mM NaCl, 4 mM KCl, 2 mM CaCl₂, 1mM MgCl₂, 5 mM HEPES, 5 mM glucose, 2 mM pyruvate and pH adjusted to 7.4 with NaOH. For whole cell current-clamp experiments, the patch pipette solution contained 140mM KCl, 7 mM NaCl, 4mM MgCl₂ 5 mM HEPES, 2 mM EGTA, 0.2 mM CaCl₂, 3mM disodium-ATP and pH adjusted to 7.3 with KOH. After establishing a tight seal the optical filter set was changed to one consisting of a blue (480nm, Chroma) bandpass interference filter (30nm bandwidth) and a dichroic mirror (570 nm). Illumination irradiance was 15W/cm² provided by a 150Watt xenon arc lamp (Optiquip M1600) gated through light source shutter (Sutter Instruments) triggered by the Axopatch controller. The relative intensity of the emitted light at the specimen plane was measured using a field stop to define the illuminated area, a hemispherical lens to dismiss steeply diverging rays, and an ILC1700w integrating sphere detector (International light) placed underneath the recording chamber. All the experiments were carried out at 25 °C.

Conclusion

COP1 may have been isolated as a retinal binding protein but it was not possible to heterologously express a functional photoreceptor-channel protein complex in either HEK293 cell or neuronal cells culture. Speculation as to how this unusual protein might be involved in the transduction process included G protein involvement²³. Although the identified algal opsins are the dominant retinal binding proteins of the algae eyespot^{18,21}, the expression of COP1 in oocytes had never shone to be functional. After our unsuccessful experiments, gene silencing experiments¹² revealed that *Chlamydomonas* transformants deprived of COP1 retained wild type photoreceptor currents, photophobic response and phototaxis proving that COP1 is not the photoreceptor for photophobic responses in *C. reinhardtii*. At this point, cDNA sequences appeared from the *C. reinhardtii* genome project, which coded for a 56 kDa Opsin type I protein (AccNo AF385748) and a 65 kDa Opsin type I protein (AccNo AF461397)

```

                                *
COP1      -MDFKSISGEYDVSKKTLKTACKLKVADNISVKLKLANPGAKPGIEVEYKGFPEATYDVKS
VOP1      MADLKNLGAEYDVTKKTLKSSCKFKVADSVGVKLKLTSPANALNVEVDGKNWGITVDVVK
BR        MLELLPTAVEGVSQAQITGRPEWIWLALGTALMGLGTLYFLVKGMGVSDPDAKKFYAITT
          *   *   *                               *   *   *   *
COP1      KDFSIEKKFKLRAGELKIKQKVPGLRTELLPSPEVQWKSHIVKGRKFSWEVEPSYCFQAR
VOP1      KDLELKGEWKLKGGEFKIKQKVPGLKTELLPSPEVQWKQHVVKNKKFAWEVEPSYCFQAR
BR        LVPAIAFTMYLSMLLGYGLTMVP-FGGEQNPIYWARYADWLFTTP--LLLLDLALLVDAD
          *   *   *                               *   *   *
COP1      KAKLDQVIELNGGKE-KLKLEFDSKLGKGLVGTTLTHKVGQSWAKQLSAKYSQAAGPSLI
VOP1      LAKLEQTVEFNGGKQ-KLKLETDSKAGVKATVGTLSAKVGNSWAKQLSVKYSKAAGPSLT
BR        QGTILALVGADGIMIGTGLVGALTKVYSYRFVWWAISTAAMLYILYVLFFGFTSKAESMR
          *   *   *                               *   #
COP1      HEVEPSKKVSLKSTVGIKARD-----LKIVALSGPMGVWIWRVK
VOP1      HEVEPSNKVSLKSTVGIKARD-----LKIVAEVKPG--KVAGVK
BR        PEVASTFKVLRNVTVVLWSAYPVVWLIGSEGAGIVPLNIETLLFMVLDVSAKVGFGLLIL

COP1      PLPAIPGKGAAPTTLVQA-----
VOP1      PKLTLEGGKVTAKAPLQPSGIIAGLSFDV-
BR        RSRAIFGEAEAPEPSAGDGAAATSD----
```

Figure 2.1 – Sequence alignment of COP1, VOP1 and Bacteriorhodopsin.

(a) Comparison of COP1 (GenBank Accession no. Z48968) sequence with VOP1 (GenBank Accession no. Z69301) and Bacteriorhodopsin (BR)(GenBank Accession no. V00474). Proposed 4 Transmembrane domains are in yellow. COP1, VOP1 homology is underlined. BR transmembrane domains are in grey. BR retinal binding domain indicated with an asterisk (*) and the retinal binding lysine is labeled with a #.

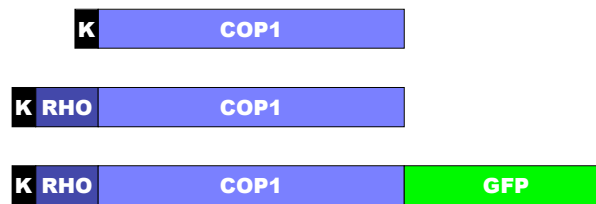


Figure 2.2 - COP1 and VOP1 cloned constructs. Constructs with fused Kozak sequence (K) and appended 39 amino acid bovine rhodopsin membrane targeting domain (Rho)²² and fluorescent protein tag GFP. The Rho tag traverses the membrane but does not include the first transmembrane domain of the bovine rhodopsin. The Rho tag should be available as an extracellular epitope for which an antibody is available for live cell immunolabeling. Use of the Rho membrane targeting domain is expected to draw the N terminal of the attached protein, COP1, through the plasma membrane orienting the N and C terminals outside the plasma membrane. The unique structure of the COP1 protein does not give any clues to the proper orientation.

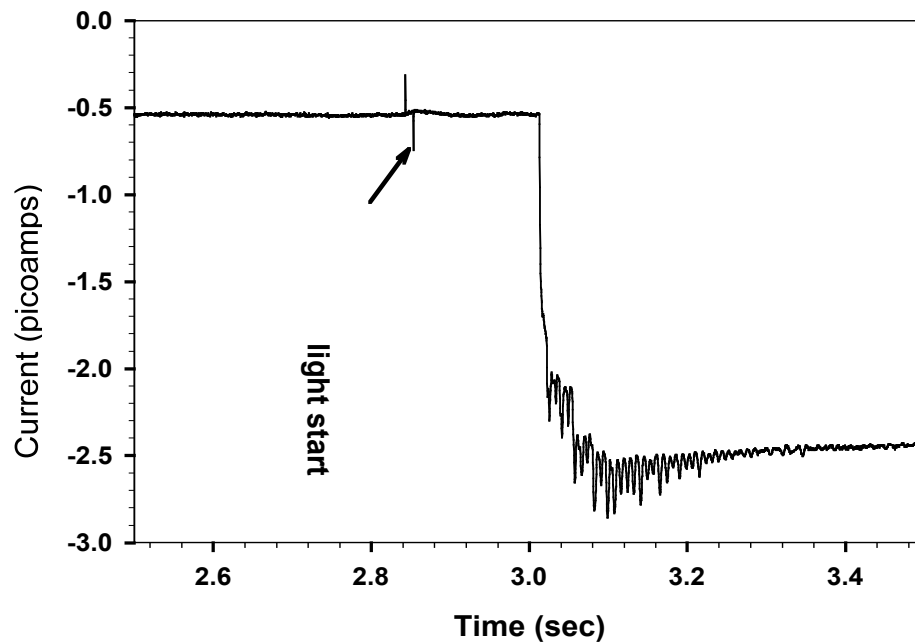
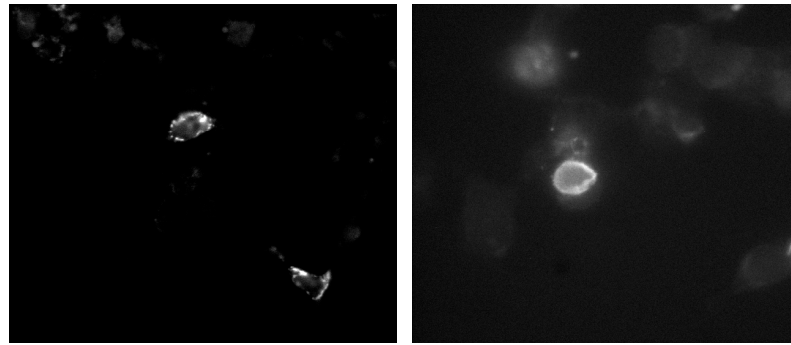


Figure 2.3 COP1 photo-current response. The only measured COP1 photo-response event showing 0.2 second delay between white light exposure and photo-response injected current measured in whole cell voltage patch clamped Rho-COP1 transfected HEK293 cell incubated overnight with supplemented 10uM all-trans Retinal DMEM media. The photocurrent delay was surmised to be due to some electronic experimental aberration due to the sharp initial transition but was never verified due to the non-reproducibility of the photo-response conditions. (Data Collected by Varda Lev-Ram)



(a)

(b)

Figure 2.4 Immunolabeling of Rho-COP1 construct expression. (a) Rho antibody live cell (non permeabilized) immunostaining of Rho-COP construct showing punctate expression on the extracellular surface of the plasma membrane (b) Rho immunostaining of Rho-COP1 construct with supplemental glycerol chaperone added to the media demonstrated increased expression on the plasma membrane though at compromised cell viability as apparent from the rounded morphology of the glycerol treated cells.

References

1. Nerbonne, J. M. Caged compounds: tools for illuminating neuronal responses and connections. *Curr. Opin. Neurobiol.* **6**, 379-386 (1996).
2. James, D. A., Burns, D. C. & Woolley, G. A. Kinetic characterization of ribonuclease S mutants containing photoisomerizable phenylazophenylalanine residues. *Protein Eng* **14**, 983-991 (2001).
3. Flint, D. G., Kumita, J. R., Smart, O. S. & Woolley, G. A. Using an azobenzene cross-linker to either increase or decrease peptide helix content upon trans-to-cis photoisomerization. *Chem Biol* **9**, 391-397 (2002).
4. Banghart, M., Borges, K., Isacoff, E., Trauner, D. & Kramer, R. H. Light-activated ion channels for remote control of neuronal firing. *Nat Neurosci* **7**, 1381-1386 (2004).
5. Katz, L. C. & Dalva, M. B. Scanning laser photostimulation: a new approach for analyzing brain circuits. *J. Neurosci. Methods* **54**, 205-218 (1994).
6. Nitabach, M. N., Blau, J. & Holmes, T. C. Electrical silencing of *Drosophila* pacemaker neurons stops the free-running circadian clock. *Cell* **109**, 485-495 (2002).
7. White, B. H. et al. Targeted attenuation of electrical activity in *Drosophila* using a genetically modified K(+) channel. *Neuron* **31**, 699-711 (2001).
8. Slimko, E. M., McKinney, S., Anderson, D. J., Davidson, N. & Lester, H. A. Selective electrical silencing of mammalian neurons in vitro by the use of invertebrate ligand-gated chloride channels. *J. Neurosci.* **22**, 7373-7379 (2002).
9. Lechner, H. A., Lein, E. S. & Callaway, E. M. A genetic method for selective and quickly reversible silencing of Mammalian neurons. *J. Neurosci.* **22**, 5287-5290 (2002).
10. Zemelman, B. V., Nesnas, N., Lee, G. A. & Miesenbock, G. Photochemical gating of heterologous ion channels: remote control over genetically designated populations of neurons. *Proc Natl Acad Sci U S A* **100**, 1352-1357 (2003).

11. Ehlenbeck, S., Gradmann, D., Braun, F. J. & Hegemann, P. Evidence for a light-induced H(+) conductance in the eye of the green alga *Chlamydomonas reinhardtii*. *Biophys. J.* **82**, 740-751 (2002).
12. Fuhrmann, M., Stahlberg, A., Govorunova, E., Rank, S. & Hegemann, P. The abundant retinal protein of the *Chlamydomonas* eye is not the photoreceptor for phototaxis and photophobic responses. *J. Cell Sci.* **114**, 3857-3863 (2001).
13. Shropshire, W. J. Phytochrome, a photochromic sensor. *Photophysiology* 33-72 (1972).
14. Foster, K. W. et al. A rhodopsin is the functional photoreceptor for phototaxis in the unicellular eukaryote *Chlamydomonas*. *Nature* **311**, 756-759 (1984).
15. Yan, B. et al. Spectral tuning in bacteriorhodopsin in the absence of counterion and coplanarization effects. *J. Biol. Chem.* **270**, 29668-29670 (1995).
16. Hegemann, P. Vision in microalgae. *Planta* **203**, 265-274 (1997).
17. Sineshchekov, O. A. & Govorunova, E. G. Rhodopsin-mediated photosensing in green flagellated algae. *Trends Plant Sci* **4**, 58-63 (1999).
18. Deininger, W., Kroger, P., Hegemann, U., Lottspeich, F. & Hegemann, P. Chlamyrodopsin represents a new type of sensory photoreceptor. *EMBO J.* **14**, 5849-5858 (1995).
19. Ebnet, E., Fischer, M., Deininger, W. & Hegemann, P. Volvoxrhodopsin, a light-regulated sensory photoreceptor of the spheroidal green alga *Volvox carteri*. *Plant Cell* **11**, 1473-1484 (1999).
20. Holland, E. M., Braun, F. J., Nonnengasser, C., Harz, H. & Hegemann, P. The nature of rhodopsin-triggered photocurrents in *Chlamydomonas*. I. Kinetics and influence of divalent ions. *Biophys. J.* **70**, 924-931 (1996).
21. Fuhrmann, M., Oertel, W. & Hegemann, P. A synthetic gene coding for the green fluorescent protein (GFP) is a versatile reporter in *Chlamydomonas reinhardtii*. *Plant J* **19**, 353-361 (1999).
22. Krautwurst, D., Yau, K. W. & Reed, R. R. Identification of ligands for olfactory receptors by functional expression of a receptor library. *Cell* **95**, 917-926 (1998).

23. Hill, K. et al. A Ca^{2+} - and voltage-modulated flagellar ion channel is a component of the mechanoshock response in the unicellular green alga *Spermatozopsis similis*. *Biochim. Biophys. Acta* **1466**, 187-204 (2000).

Chapter 3

Heterologous Expression of Functional Light Activated Algae Channels

Introduction

Upon completion and publication of the Kazusa Chlamydomonas Reinhardtii Genome project (<http://www.kazusa.or.jp>), two proteins were classified as a 56kDa Opsin type I protein (AccNo AF385748) and a 65kDa Opsin Type I protein (AccNo AF461397). These two proteins had some amino acid sequence homology to archaeal sensory rhodopsins, specifically amino acids that defined the retinal binding site and the ion conducting channel core were conserved. The N terminal domain of the two purported algae channel opsin protein sequences, channel opsin 1 (ChOP1) and channel opsin 2 (ChOP2), were aligned and modeled using the Protein Data Base (PDB) bacteriorhodopsin structure¹ as a template and were found to have high secondary structure homology to bacteriorhodopsin (BR) (fig 3.1). The C terminal domains of both ChOP1 and ChOP2 have unknown functions.

The in-vivo photocurrent amplitude response curves were reported to be biphasic². A model was proposed consisting of a slower low light saturating response current and a faster high-light-saturating response current^{3,4}. In an in-vivo cell population assay that monitors the differential response of cells facing the light versus cells facing away from the light, the authors demonstrated that both ChR1 and ChR2 (ChOP1 and ChOP2 apoprotein respectively + retinal chromophore) contributed to the photoreceptor currents

³. From experiments on *C. reinhardtii* ChOP1 and ChOP2 RNAi knockouts, it was observed that ChR1-deprived cells had reduced photocurrents at high flash intensities, whereas in ChR2-deprived cells had reduced photocurrents at low flash energies. The authors concluded that ChR1 elicits the high-intensity response, whereas ChR2 is responsible for low-intensity photocurrents ³. The mechanism as to how and to what extent ChR1 and ChR2 evoke photo-attraction and photo-phobic responses of phototaxis could not be resolved. ChR1 and ChR2 may only be a step in a signal transduction pathway of phototaxis in *C. reinhardtii*. Early on, the photocurrent attributed to ChR2 was described as slow and, in analogy to phototaxis in archaea, coupling of a ChR2 to a specific transducer was proposed. The fast response of ChR1 resembled the archaeal response and the possibility that ChR1 might be an ion channel by itself was the most likely possibility ³. The two proteins revealed in the Kazusa *C. reinhardtii* EST genome project, here referred to as ChOP1 and ChOP2⁵, alluded to as chlamyopsins Cop3 and Cop4 ⁶, but originally characterized as CSOA and CSOB ³ and later as Acop-1 and Acop-2 ⁷, are the photo-channels responsible for the high light intensity fast photocurrent response and the low intensity slow photophobic-current response respectively.

Microbial Rhodopsins: Archaeal Rhodopsin Homologs

There are hundreds of photochemically reactive proteins found in both prokaryotes and eukaryotes, that use vitamin-A aldehyde (retinal) as their chromophore. Retinylidene proteins (rhodopsin) play multiple roles in

organisms such as the photoreceptor for vision and a regulator of circadian rhythms and melatonin production. In *C. reinhardtii*, a flagellated eukaryotic alga, It has been known from behavioral action spectrum assay observations that a rhodopsin serves as the photoreceptor pigment for phototaxis ⁸.

Common among these rhodopsins is the formation of an interior retinal chromophore binding pocket in the hydrophobic core of 7 transmembrane helices. Rhodopsins can be classified into 2 distinct types of rhodopsins.

Type 1 archaeal rhodopsins function as light driven ion transporters and phototaxis sensory rhodopsins.

Type 2 sensory rhodopsins consist of photoreceptor proteins in animal eyes. Included in this type of retinylidene proteins are visual pigment receptor proteins in the pineal gland, hypothalamus and other tissues of lower vertebrates, extra-ocular retinal photoisomerases, and encephalopsin (found in human and mouse brains). All type 2 rhodopsins are reported only in higher eukaryotes.

Type 1 archaeal rhodopsins

The light driven ion pumps bacteriorhodopsin ⁹ and halorhodopsin ^{10,11} and the phototaxis receptor sensory rhodopsin I ¹² and sensory rhodopsin II ¹³ were the microbial rhodopsin extensively studied before 1999. Both BR and HR hyperpolarize the membrane to generate a positive outside membrane

potential thereby creating inwardly directed proton motive force. Microbial sensory rhodopsins SRI and SRII are phototaxis receptors controlling the cells swimming behavior in response to changes in light intensity and color. In proteins that form microbial pigments, the retinal chromophore is attached by a protonated Schiff linkage to a lysine in the binding pocket. Photoisomerization of the retinal initiates the photochemical reactions. In bacteriorhodopsin, retinal photoisomerizes from its all *trans* to its 13-*cis* form¹⁴ and triggers the translocation of one proton from the cytoplasmic side of the membrane to the extracellular side¹⁵. After executing this function, the 13-*cis* retinal isomer spontaneously reverts back to all-*trans* retinal, and the photocycle is again prepared for photostimulation.

Heterologous expression of ChOP1 and ChOP2, at the onset, had not been reported and the primary mode of action for phototaxis remained obscure. We aimed to express ChOP1 and ChOP2 in mammalian cells in the hope of obtaining a functional rhodopsin and possibly allow us to determine its action spectrum. With this knowledge applied to neuronal systems we could achieve the ends of remote optical stimulation of neurons for neuronal mapping and in-vivo studies in relation to cognitive function of the brain.

Results and Discussion

The two *C. reinhardtii* Type I opsins nucleotide sequences were available from Kazusa but the actual clones were not available and therefore it was of foremost importance to extract and clone the genes from *C. reinhardtii*

cells. The *C. reinhardtii* cells from which the total mRNA was extracted were grown under conditions, provided by Kazusa, which included full room light and constant agitation at room temperature. Cells grown in the dark did not produce the opsins necessary for phototaxis because it was not a necessary response of the cells. Interestingly, the cells never developed flagella because the constant agitation and adequate light made the flagella unnecessary. The ChOP1 and ChOP2 cDNAs were isolated by PCR directly from the *C. reinhardtii* total mRNA extraction and subcloned into mammalian expression vector pCDNA3 (Invitrogen). To improve plasma membrane targeting, I initially fused the 39 N terminal amino acids of bovine rhodopsin, a plasma membrane localization tag (Rho)¹⁶, to the N terminal of the ChOP1 gene making the fusion protein Rho-ChOP1 (fig 3.2b).

Preliminary, proof of concept, whole cell depolarization experiments with ChOP1 heterologously expressed in HEK293 cells were conducted prior to attempting functional expression of ChOP1 and ChOP2 rhodopsin in neuronal cultures. The Rho-ChOP1 construct was co-transfected with GFP into HEK293 cells. Cells were incubated for 12 hours, in Dulbecco's Modified Eagle's Medium (DMEM) with 10% Fetal Bovine Serum (FBS), 1% penicillin/streptomycin, and 1 μ M all-trans retinal (Sigma), in the dark to avoid channel activation and eventual cell mortality. GFP fluorescent cells were whole cell patched but did not exhibit any photoactivatable currents.

I fused GFP to the C terminal of the Rho-ChOP1 construct to directly track the expression of Rho-ChOP1 (fig 3.2c). This GFP fusion construct was

transiently transfected into HEK293 cells. Fluorescent imaging indicated that much of the construct expression was retained in the Endoplasmic reticulum (ER), however, there also appeared to be significant membrane expression (fig 3.3). Fluorescent cells were whole cell patch clamped by Dr. Oded Tour but did not exhibit any photoactivated currents. On the assumption that reducing the ER retention would increase membrane expression, hence, increase the photo-current, an ER export tag (FCYENE)¹⁷ was appended to Rho-ChOP1 (fig 3.4c). Immunostaining of the fixed and permeabilized cells indicated no appreciable increase of plasma membrane expression.

Without being able to successfully measure any heterologously expressed ChOP1 channel photocurrents, we turned our attention to the orientation of the expressed ChOP1 protein in the membrane. The fact that the C terminal GFP fusion is fluorescent on the Rho-ChOP1-GFP construct expression did not indicate the orientation of the protein in the membrane. The GFP can fluoresce if it is cytosolic expressed or extracellularly translocated. Using bacteriorhodopsin as a model we would expect that the N terminal of the ChOP1 protein to be extracellular making the C terminal of the seven transmembrane channel cytosolic. The Rho tag proves plasma membrane localization as was verified with live cell (non permeabilized) immunostaining with a Rho antibody (fig 3.5b) establishing that the 39 amino acid epitope was extracellular. It was not clear if the Rho tag interfered with the translocation of the first transmembrane domain of the ChOP1 channel from extracellular to intracellular, as would be expected from the bacteriorhodopsin model. I

genetically added a FLAG epitope tag to the C terminal of the Rho-ChOP1 construct. Transiently transfected HEK293 cells expressing the Rho-ChOP1-FLAG construct were permeabilized, fixed with paraformaldehyde and immunolabeled with a FLAG antibody to confirm the location of the C terminal to be cytosolic. The non-permeabilized cells are not immunolabeled. It can be concluded that the C terminal of ChOP1 is cytosolic (fig 3.5a).

I fused the FLAG epitope tag to the C terminus of ChOP1 protein alone, without the Rho membrane targeting domain to determine if the ChOP1 channel protein alone with a Kozak sequence can be folded correctly when expressed heterologously (fig 3.4b). I expressed ChOP1-FLAG construct in HEK293 cells and immunolabeled with FLAG antibody with a conjugated fluorophore. Fluorescent images of immunolabeled permeabilized cells clearly indicated that ChOP1-FLAG was expressed on the plasma membrane (fig 3.6a). The C terminal of ChOP1 was verified cytoplasmic because no significant FLAG immunolabeling was apparent in fixed nonpermeabilized cells (fig 3.6c).

The FLAG immunostaining of the ChOP1-FLAG construct in permeabilized cells demonstrated a surprising amount of membrane staining. The absence of a Rho tag was verified by the lack of Rho immunostaining on live cells (fig 3.6b). The question is raised as to the necessity and the consequence of the Rho tag on the function of the ChOP1 channel. I removed the FLAG epitope tag and fused a GFP reporter to the C terminus of the ChOP1 protein and transfected HEK293 cells with the stripped down

construct. The membrane expression of ChOP1-GFP was surprisingly significant without the Rho tag. Dr. Oded Tour whole cell patch clamped several fluorescent cells but did not measure any photoactivatable currents.

At this point in time, I had tested many different heterologously expressed ChOP1 channel configurations and none formed a functional channel. Perhaps the channel was not being translated properly and that the ChOP1 gene codon sequence needed to be humanized for heterologous expression to produce a functional channel. The literature reported that the ChOP1 channel had been tested in oocytes and found to be a proton channel with low conductance at neutral extracellular pH. The fact that it was a proton channel reduced the appeal of the channel for stimulating neurons in that the conductance was low and changing the cytosolic pH of the neuron might stimulate it but it could also have other undesirable and unpredictable consequences. At this point we questioned the feasibility of the project and decided it was no longer a priority. ChOP2 remained untested.

Others then reported heterologously expressed ChOP2 channels in oocytes with measured light induced cation currents¹⁸. I cloned the fluorescent protein, mCherry, to the C terminal of the seven transmembrane retinal binding ion channel domain of ChOP2 (nucleotides 1 - 945) into the mammalian expression vector pCDNA3 (fig 3.7a). I expressed this ChOP2-mCherry in HEK293 cells and fluorescent imaging revealed red fluorescent membrane targeting and no ER retention. The fluorescent HEK293 cells were whole cell patch clamped by Dr. John Lin. Light activated currents were

observed in transfected cells. Surprisingly photo currents were observed in cells with and without supplemental $10 \mu\text{M}$ all-trans retinal, however, untransfected cells exhibited no photocurrent responses (fig 3.7b). It was assumed that the media likely contained retinal or a vitamin A derivative that was allowing activation of all transfected cells. To confirm this assumption, I transfected the ChOP2-mCherry construct into HEK293 cells grown in minimal media (without fetal bovine serum). The ChOP2-mCherry transfected HEK293 cells continued to exhibit a photoactivatable response. We concluded that the HEK293 cells themselves are producing enough retinal to provide a chromophore for the ChOP2.

The response characteristics (temporal and spectral) of the photochannel currents with supplemental retinal are identical when compared to photochannel currents in cells without supplemental retinal added. Here we have demonstrated but not characterized the ChOP2 channel. The literature reports the heterologously expressed cation channel inward photocurrents characterized in oocytes¹⁸. The photocurrent was found to be inversely proportional to the cation atomic radius and is preferentially permeable to the divalent cation calcium with an estimated inward current of 200pA at -100mV membrane potential.

Channel closing is pH dependent and occurs coincident with termination of exposure to light with a 60msec time constant at physiological pH. Channel closure is a multi step dynamic and is a function of intracellular pH in that a lower pH slows channel closing kinetics. Protonation of

extracellular residues, however, have been proposed to facilitate channel recovery between light exposure episodes¹⁸. Closing rates down to 10msec are typical. If the ChOP2 channel functions similarly in neurons, these results would indicate that neuron depolarization and activation should be possible.

The ChOP2-mCherry construct was transiently transfected into neurons supplemented with 1 μ M all-trans retinal. Neurons were incubated overnight in the dark and whole cell voltage clamped to –60 mV. The neurons exhibited a photocurrent response on the order of picoamps and in the submillisecond time frame. (fig 3.8).

Materials and Methods

C. reinhardtii Strains

C reinhardtii strain supplied by S. Mayfield lab (The Scripps Research Institute La Jolla, CA) were grown in low light conditions in TAP (Tris-acetate-phosphate medium) at 30°C with continuous shaking. After 3 days incubation, The cells were centrifuged and transferred to denaturing lysis buffer containing a nonionic detergent .To disrupt the cell walls, the sample is homogenized by repeatedly passing the lysate through a 20 gauge needle and syringe. Centrifugation separated nuclei and cell debris from the cytoplasm. The supernatant is buffered in a solution containing guanidine isothiocyanate (GITC) for 1 hour to inactivate RNAses. Ethanol is added to the homogenized lysate to condition the RNA to adhere to the silica-gel column. Total RNA is

bound to the column and then washed with a high salt buffer and eluted with Rnase free water.

Full length ChOP1 and ChOP2 cDNA was isolated from *C. reinhardtii* cell total mRNA by PCR using the ChOP1 primers 5'-GCGCGCAAGCTTGCCACCGAGGAGGACGACGAGACG-3', and 5'-GCGCGAATTCGCTGCTCTCCGTCTCGTCGTCCTCCTC-3' and the ChOP2 primers 5'-GCGCGCAAGCTTGCCACCATGGATTATGGAGGCGCCCTGAGT-3' and 5'-GCGCGAATTCGCTGCTCTCGTACTTGCCGGTGCCCTTGTG-3'. Primers were designed from gene sequences revealed by the *C. reinhardtii* genome sequencing project at Kazusa DNA Research Institute (<http://www.kazusa.or.jp/>).

Cell Culture

HEK293T (ATCC) cells were cultured in DMEM (Dubco) supplemented with 10% fetal bovine serum and 1% penicillin/streptomycin (enriched DMEM). The cells were grown for 24 hours to approximately 40% confluence, transiently transfected using FuGENE 6 (Roche) and examined 24 hours to 48 hours after transfection. The Cell media was replaced 12 hours post FuGENE transfection with enriched DMEM supplemented with 1 μ M all trans retinal. Stable HEK293 cells were selected with 1 μ g/ml G418 (Invitrogen) and maintained with 600 ng/ml G418. Cells were grown to 80% confluence and passed 3 times before sorting for GFP fluorescence on Becton Dickinson FACS-Vantage DiVa flow cytometer.

ChOP1 and ChOP2 Constructs

Escherichia coli DH5 α was used for cloning the genes from the extracted cDNA. *E. coli* transformants were grown in Luria-Bertani (LB) medium in the presence of ampicillin (50ug/ml) at 37°C. The full length ChOP1 and ChOP2 were expressed in mammalian cells using the pCDNA3 (Invitrogen) expression vector. The N terminal 346 amino acids of ChOP1 and the 315 amino acids of Chop2 are gene fragments corresponding to the seven transmembrane rhodopsin channel domain. I cloned the gene fragments into the HindIII and EcoRI restriction sites of pCDNA3 expression vector using the PCR product of the cDNA N terminal primers, which include a HindIII restriction site and a start Kozak sequence. The ChOP1 346 truncation reverse primer includes an appended termination codon, TAA, and EcoRI restriction site, 5'-GCGCGAATTCTTACAGGATGGCGTGGGCGATG-3'. The ChOP2 315 truncation reverse primer with an appended termination codon, TAA, and EcoRI restriction site is 5'-GCGCGAATTCGCTGCTCTCGTACTTG CCGGTGCCCTTGTG-3'. All construct sequences were sequenced and confirmed to published data base sequences.

For verification of membrane expression, various fluorescent proteins were appended to the rhodopsin channel gene fragments. The fluorescent proteins are all terminated with the same nucleotides and so the cloning is identical regardless of the FP. The restriction sites EcoRI and XhoI were added to the FPs N and C terminals respectively by PCR using the forward primer 5'-GCGCGAATTCGCCACCATGGTGAGCAAGGGCGAG-3' and the reverse primer 5'-GCGCGCGGCCGCTTACTTGTACAGCTCGTCCA-3'. The

PCR is digested with EcoRI and XhoI and subcloned into the MCS of pCDNA3. The FP sub clone vector is digested with HindIII and EcoRI to prepare it for the channel rhodopsin insert. The ChOP1 and ChOP2 inserts are prepared by PCR from the full length channel clones with a C terminal ESS flexible linker using the primers 5'-GCGCGCAAGCTTGCCACCATGTCGCGGAGGCCATGG-3' and 5'-GCGCGAATTCGCTGCTCTCCGTCTCGTCGTCCTCCTCGTGAC-3' for ChOP1-346 and for ChOP2-315, 5'-GCGCGCAAGCTTGCCACCATGGATTATGGAGGCGCC-3' and the 315 amino acid reverse primer 5'-GCGCGAATTCTTAGTACTTGCCGGTGCC-3'. The PCR product of both ChOP1-346 and ChOP2-315 amino acid rhodopsin channels are ligated into the FP subclone and then amplified.

Hippocampal cell culture

Hippocampi primary cells were prepared, cultured and transfected by Samuel Andrew Hires using postnatal day 0 Sprague-Dawley rats were removed and treated with papain (20U/ml) for 45 min at 37°C. The digestion was stopped with 10ml of MEM/Earle salts without l-glutamine along with 20mM glucose, serum extender (1:1000), and 10% heat inactivated fetal bovine serum containing 25mg of bovine serum albumin (BSA) and 25mg of trypsin inhibitor. The tissue was triturated in a small volume of this solution with a firepolished Pasteur pipette, and ~10000 cells in 1ml plated into astrocyte feeder wells prepared a few days earlier in 24 well plates. Cells were plated in culture medium: Neurobasal containing 2X B-27 (life technologies) and 2 mM Glutamax-I (life technologies). The culture medium supplement B-

27 contains retynyl acetate, but no B-27 was present during recording and no all trans retinal was added to the culture medium or recording medium for any of the experiments described. One-half of the medium was replaced with culture medium the next day, giving a final serum concentration of 1.75%

Neuronal primary culture transfection

Hippocampal cultures were transfected on day 7 in vitro using calcium phosphate. A 25 μ l per well mixture of DNA and CaCl_2 (0.25M) was added dropwise to 25 μ l per well of 2X HBS to form a precipitate at room temperature after 20 minute incubation. 50 μ l per well of the precipitate was added to Hippocampal cultures seeded in 24 well plates and then incubated at 37°C for 90 minutes. Removed the calcium phosphate/DNA precipitate. The cells were then osmotically shocked with HBS (5% glycerol, APV (5mM), Kynurenate (100mM), MgCl_2 (100mM) in HEPES pH7.5) for 1-2 minutes. Washed the cells 3 times with culture media and then returned the coverslips back to the saved conditioned media. Returned the cells to the incubator for 3 days before experiments.

Microscopy and Electrophysiology (HEK293 Cells)

Whole-cell patch-clamp recordings were performed by Dr. Varda Lev-Ram and Dr. John Lin using ChR2 expressing HEK293 cells visually identified under conventional epifluorescent microscopy (Diaphot microscope, Nikon) equipped with a 40X, 1.3 NA oil objective lens (40x /1.3NA Fluor, Nikon), using a conventional patch clamp system (Axopatch 200A plus Digidata1200, Molecular Devices Co.). The bath solution contained 140mM NaCl, 4 mM KCl,

2 mM CaCl₂, 1 mM MgCl₂, 5 mM HEPES, 5 mM glucose, 2 mM pyruvate and pH adjusted to 7.4 with NaOH. For whole cell current-clamp experiments, the patch pipette solution contained 140 mM KCl, 7 mM NaCl, 4 mM MgCl₂, 5 mM HEPES, 2 mM EGTA, 0.2 mM CaCl₂, 3 mM disodium-ATP and pH adjusted to 7.3 with KOH. After establishing a tight seal the optical filter set was changed to one consisting of a blue (480 nm, Chroma) bandpass interference filter (30 nm bandwidth) and a dichroic mirror (570 nm). Illumination irradiance was 15 W/cm² provided by a 150 Watt xenon arc lamp (Optiquip M1600) gated through light source shutter (Sutter Instruments) triggered by the Axopatch controller. The relative intensity of the emitted light at the specimen plane was measured using a field stop to define the illuminated area, a hemispherical lens to dismiss steeply diverging rays, and an ILC1700w integrating sphere detector (International Light) placed underneath the recording chamber. All the experiments were carried out at 25 °C.

Microscopy and Electrophysiology (Neurons)

Cultured hippocampal neurons were recorded at approximately DIV 6 (2 days post transfection). Neurons were recorded by means of whole-cell patch clamp, using Axon Multiclamp 700B (Axon Instruments) amplifiers on an Olympus inverted scope equipped with a 20x objective lens. Borosilicate glass (Warner) pipette resistances were ~4 M Ω . Access resistance was 10-30 M Ω and was monitored throughout the recording. Intracellular solution consisted of (in mM) 97 potassium gluconate, 38 KCl, 0.35 EGTA, 20 HEPES, 4

magnesium ATP, 0.35 Sodium GTP, 6 NaCl and 7 phosphocreatine (pH7.25 with KOH). Neurons were recorded in Tyrode solution (above). All experiments patched fluorescent cells immersed in Tyrode solution containing 5 μ M NBQX and 20 μ M gabazine to block synaptic transmission. Photocurrents were measured while holding neurons in voltage clamp at -100mV. Recovery from inactivation was measured by measuring photocurrents while illuminating neurons with pairs of 500 ms denaturation light pulses, separated by periods of darkness lasting 1-10sec.

PClamp 9 software (Axon Instruments) was used to record all data, and a DG-4 high speed optical switch with a 150Watt xenon arc lamp (Optiquip M1600) gated through light source shutter (Sutter Instruments) triggered by the Axopatch controller was used to deliver the light pulses for ChOP2 activation. A GFP filter set with an excitation filter of 470nm with a 40nm bandwidth with (Chroma) a dichroic 495nm long pass (Chroma) was used for delivering the blue light for ChOP2 activation. YFP was visualized with a standard YFP excitation filter set of 500nm with a 20nm bandpass (Chroma) and a dichroic 515nm long pass (Chroma) and an emission 535nm with a 30nm bandwidth (Chroma). Through a 20X objective lens, the power density of the blue light was 15 W/cm². The relative intensity of the emitted light at the specimen plane was measured using a field stop to define the illuminated area, a hemispherical lens to dismiss steeply diverging rays, and an ILC1700w integrating sphere detector (International light) placed underneath the recording chamber.

Pulse series was synthesized by pCLAMP8 software and then exported through clamp 9 via a Digidata board (Axon) attached to a PC. All the experiments were carried out at 25 °C.

Conclusion

Genetically encoded, light activated ion channels from algae are a noninvasive approach to subsecond control of the electrical activity of targeted neurons. Previous described photostimulation methods have proved useful but cumbersome as a way to noninvasively stimulate neuronal populations. Unlike animal photoreceptors, simpler organisms, such as algal photoreceptors are reported to be simple single subunit light gated cation channel that respond with subsecond kinetics to initiate phototaxis. The primary algal photoreceptor protein ChOP1 and ChOP2 have been cloned from DNA derived from *C. reinhardtii* whole cell mRNA extraction and expressed heterologously in mammalian cells and neurons. ChOP1 is a purported proton channel and experiments initially never produced functional light activated channels with our system. Further pursuit of a functional ChOP1 channel was abandoned due to the dubious utility of a proton channel as a way to stimulate neurons. We have demonstrated functional ChOP2 photo-channels and successfully depolarized cells upon stimulation with incident 470nm light.

ChOP2 photo-channels in cultured neurons show a response though the algae apoprotein heterologous expression produced a photo-response, it

could be beneficial to humanize the codon sequence. There are many possible *in-vivo* applications for the ChOP2 photo-channel. We can use specific neuron subpopulation expression promoters to understand precisely which cell types contribute to functional control. Recently, optophysiological stimulation using ChOP2 expressed ectopically in blind mouse retina has restored light sensitivity¹⁹ and in drosophila larvae, ChOP2 ectopical expression has substituted light as a stimuli during olfactory learning²⁰.

There are some limitations to the ChOP2 system, as it exists for neuronal circuit experimentation, primarily that the penetration depth of the light stimulus is limited by the scattering characteristic of the tissue and therefore is limited, at the ChOP2 stimulation wavelength, to a superficial 2um. To facilitate deeper stimulus penetration depths, a clue can be taken from two photon microscopy by creating constructs with a red shifted action spectrum to the near IR (640nm) for greater tissue penetration. Creating constructs with a shifted stimulation wavelength will also facilitate multi-cell stimulation within a single microscope field adding to the utility of the light-activated channel. Random mutagenesis, and DNA shuffling of the Channel protein is proposed to create a diverse cDNA library. Considerable mutagenesis and selection may be required to achieve functional proteins with an optimum shifted action spectrum and an appropriate photoreceptor current response fidelity to depolarize cells. Expression of the library in mammalian cells and subsequent selection of the optimized photoreceptor/channels may be achieved using

existing fluorescent calcium or voltage indicators with conventional flow cytometry or fluorescence activated cell sorting.

Using BR as a model, changes in the amino acid residues have an affect on the action spectrum of the rhodopsin but we can only expect approximately a 100nm red shift from known BR variants. A second approach is to change the chromophore. Experiments have been done in the past on *C reinhardtii* cells where the all trans retinal was replaced with synthesized retinal analogs and have achieved activation spectral shifts to 660nm in-vivo (K.W. Foster, personal communication). This combined with apoprotein mutagenesis may accomplish the goal of shifting the channel action spectrum while retaining the channel functionality.

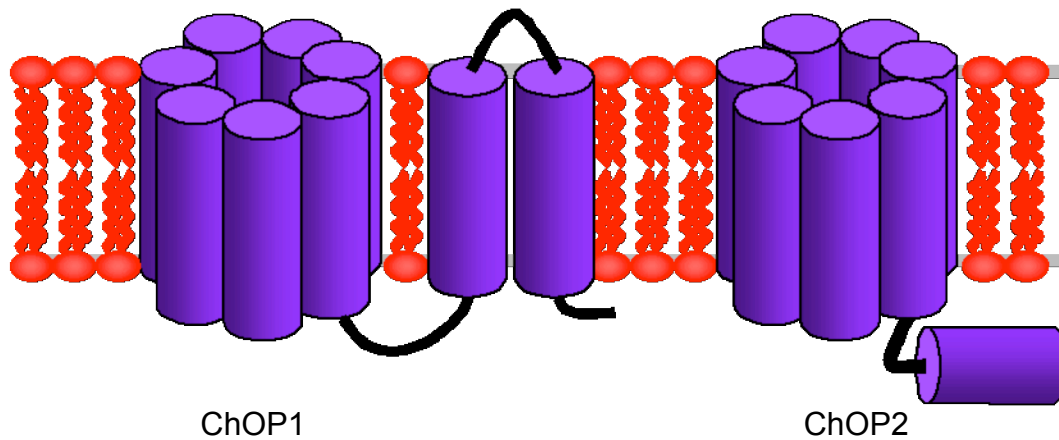


Figure 3.1 ChOP1 and ChOP2 channel secondary structure. Full length channel opsin secondary structure domains. N terminal domains are modeled to BR and the C terminal domains are of unknown function.

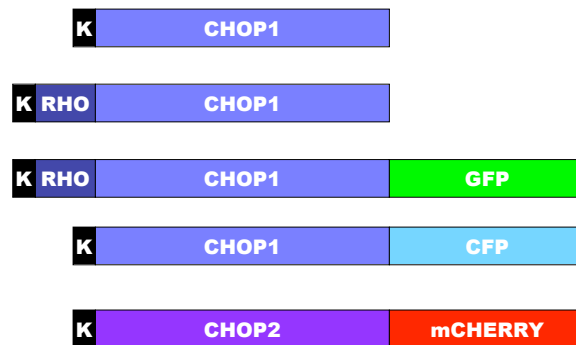


Figure 3.2 ChOP1 and ChOP2 cloned constructs. All constructs have N terminal Kozak sequence for mammalian expression. First 39 amino acids of the Bovine rhodopsin (Rho) was appended to the N terminal of ChOP1 for enhanced membrane expression. The Rho membrane targeting domain was removed for fear of channel functional interference. Fluorescent proteins were fused to the C terminus for membrane expression verification and proved to not be a hindrance to channel function.

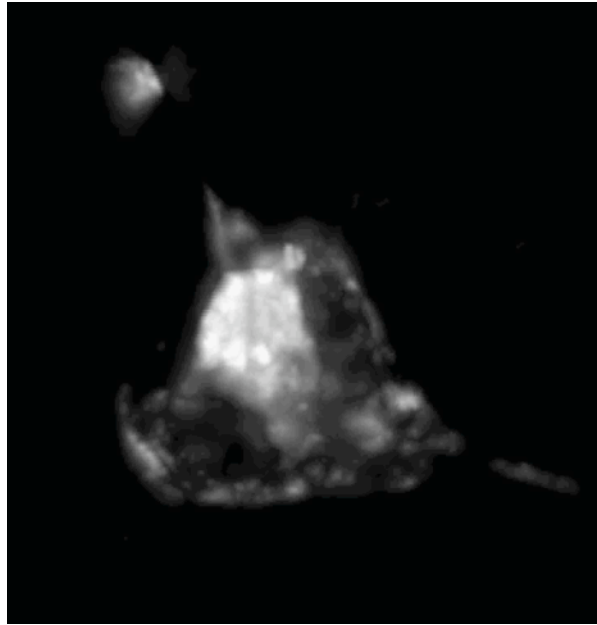


Figure 3.3 Rho-ChOP1-GFP heterologously expressed in HEK293 cells. Fluorescent image of Rho-ChOP1-GFP construct has significant membrane expression but also exhibited significant endoplasmic reticulum retention. Despite membrane expression, ChOP1 expressing HEK293 cells supplemented with retinal demonstrated no photo-induced channel currents.



Figure 3.4 ChOP1 with fused FLAG epitope and ER export Tags. ChOP1 appended with Rho and FLAG epitope tags to verify protein orientation and expression levels on the plasma membrane.

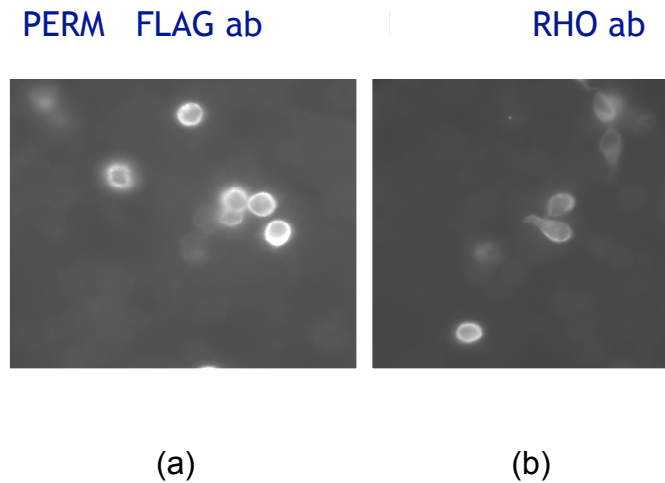


Figure 3.5 Rho-ChOP1 construct orientation of membrane expression. (a) Fluorescent image of fixed and permeabilized HEK293 cells expressing Rho-ChOP1-FLAG immunostained with FLAG antibody showing high plasma membrane expression. Cells appear to be rounding up, high membrane expression could compromise the cell health hence morphology. (b) Fluorescent image of fixed permeabilized HEK293 cells expressing Rho-ChOP1-FLAG immunostained with Rho antibody showing high plasma membrane expression.

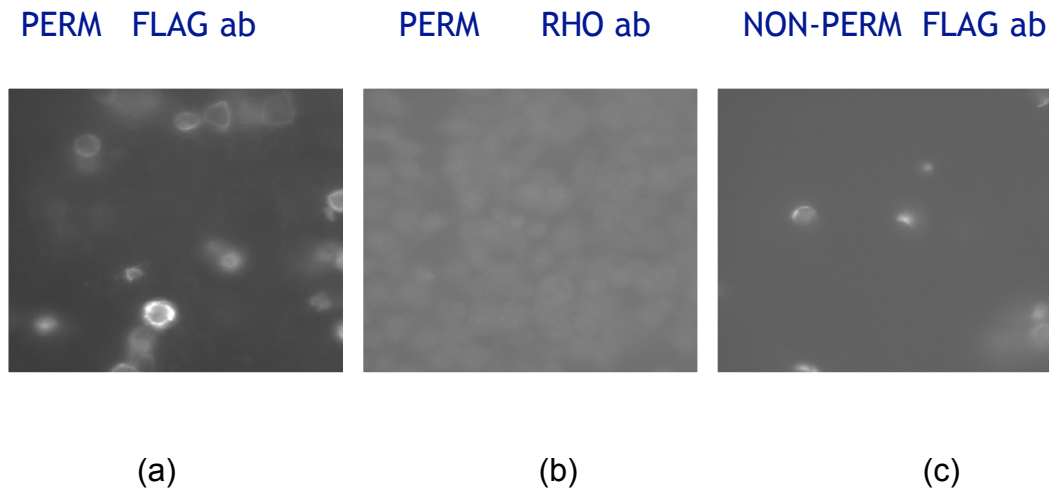


Figure 3.6 ChOP1 construct orientation of membrane expression.
 (a) ChOP1-FLAG expression without Rho tag on fixed permeabilized cells and stained with FLAG antibody showing high expression plasma membrane targeting of ChOP1 channel protein (b) ChOP1-FLAG expressed without Rho tag in fixed permeabilized HEK293 cells verifying no presence of Rho membrane targeting domain. (c) Non-permeabilized HEK293 cells expressing ChOP1-FLAG confirming that C terminus is expressed intracellularly. Some FLAG immunostaining of the C terminal epitope was apparent because the fixing process somewhat permeabilized the cells.

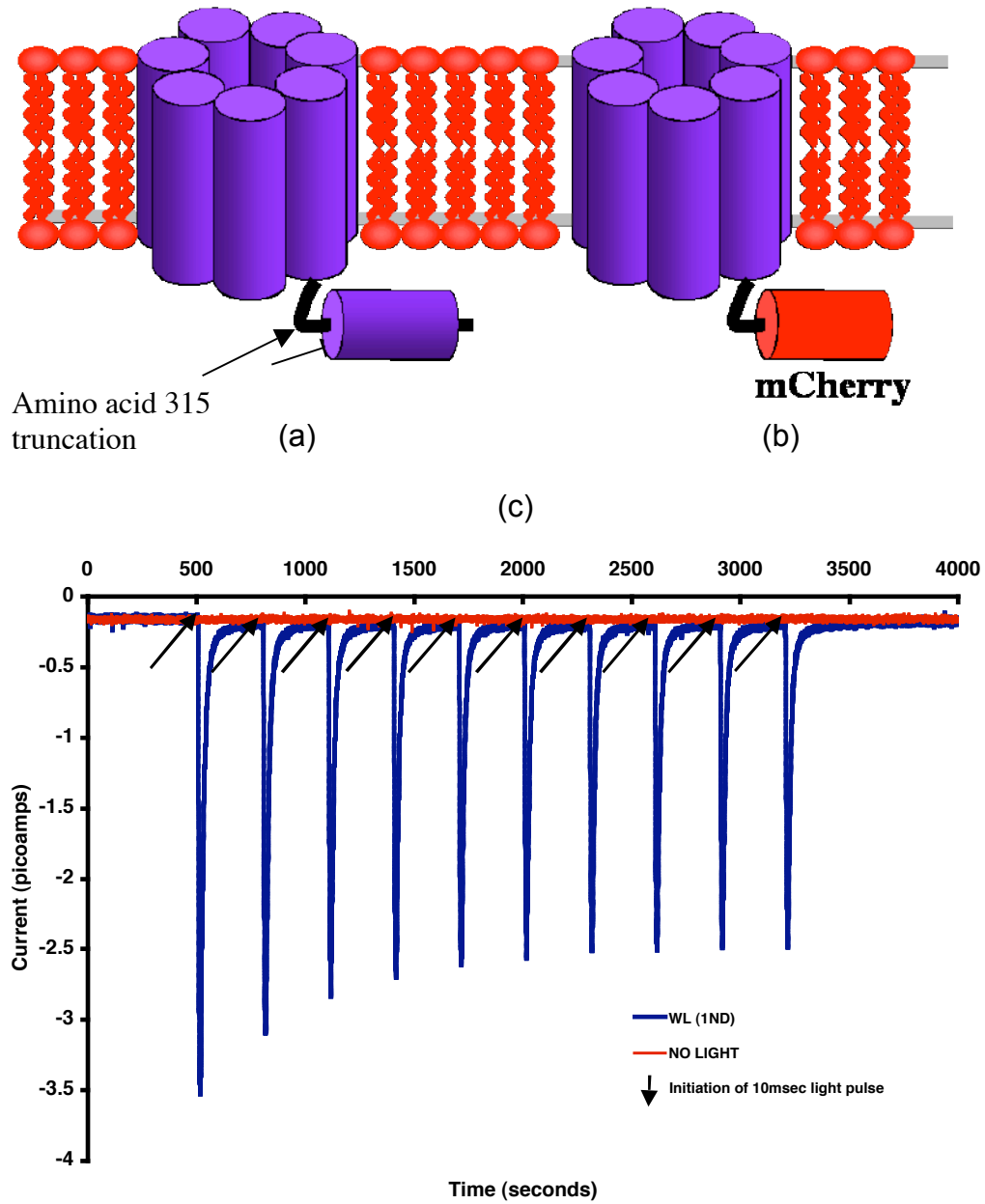


Figure 3.7 ChOP2 channel construct and response. (a) Full length ChOP2 membrane and (b) ChOP2-mcherry construct. (c) Light activated response of ChOP2-mcherry in HEK293 cells. Untransfected cells have no photoinduced currents (Varda Lev-Ram).

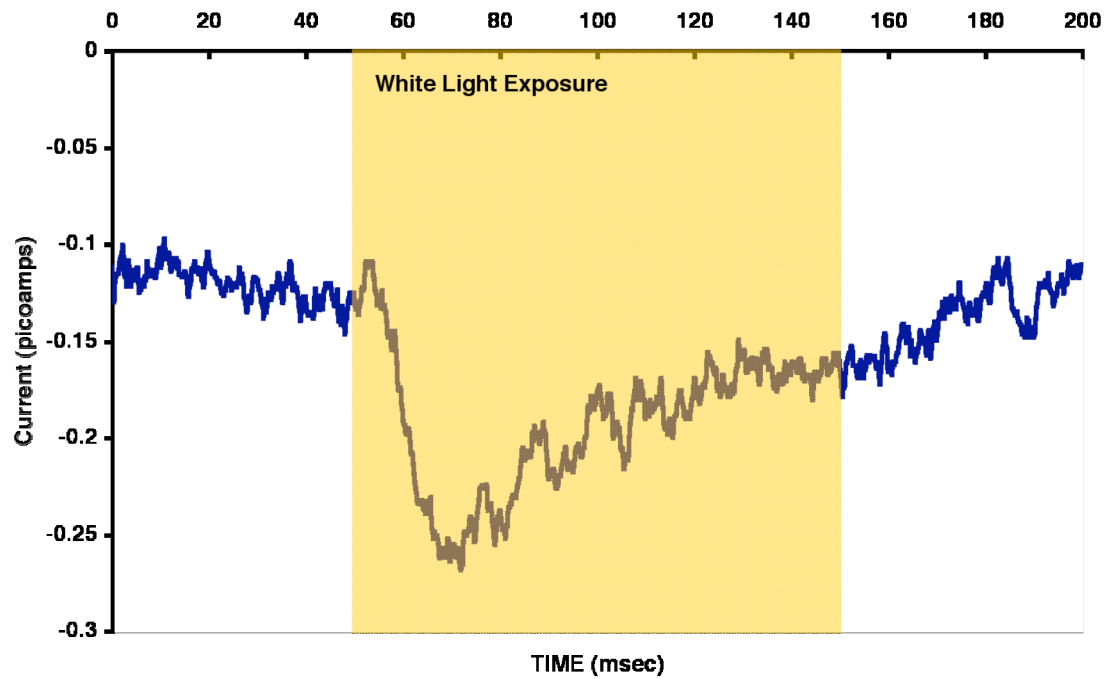


Figure 3.8 ChOP2 channel neuronal response. Light –induced inward current of neurons transiently transfected neurons with ChOP2-mCherry and supplemented with 1 μ M retinal for 1 hour prior to experiment. (Varda Lev Ram)

References

1. Subramaniam, S. & Henderson, R. Crystallographic analysis of protein conformational changes in the bacteriorhodopsin photocycle. *Biochim. Biophys. Acta* **1460**, 157-165 (2000).
2. Sineshchekov, O. A., Govorunova, E. G., Der, A., Keszthelyi, L. & Nultsch, W. Photoinduced electric currents in carotenoid-deficient *Chlamydomonas* mutants reconstituted with retinal and its analogs. *Biophys. J.* **66**, 2073-2084 (1994).
3. Sineshchekov, O. A., Jung, K. H. & Spudich, J. L. Two rhodopsins mediate phototaxis to low- and high-intensity light in *Chlamydomonas reinhardtii*. *Proc Natl Acad Sci U S A* **99**, 8689-8694 (2002).
4. Ehlenbeck, S., Gradmann, D., Braun, F. J. & Hegemann, P. Evidence for a light-induced H(+) conductance in the eye of the green alga *Chlamydomonas reinhardtii*. *Biophys. J.* **82**, 740-751 (2002).
5. Nagel, G. et al. Channelrhodopsin-1: a light-gated proton channel in green algae. *Science* **296**, 2395-2398 (2002).
6. Hegemann, P., Fuhrmann, M. & Kateriya, S. Algal Sensory Photoreceptors. *Journal of Phycology* **37**, 668-676 (2001).
7. Suzuki, T. et al. Archaeal-type rhodopsins in *Chlamydomonas*: model structure and intracellular localization. *Biochem. Biophys. Res. Commun.* **301**, 711-717 (2003).
8. Foster, K. W. et al. A rhodopsin is the functional photoreceptor for phototaxis in the unicellular eukaryote *Chlamydomonas*. *Nature* **311**, 756-759 (1984).
9. Oesterhelt, D. & Stoeckenius, W. Functions of a new photoreceptor membrane. *Proc Natl Acad Sci U S A* **70**, 2853-2857 (1973).

10. Matsuno-Yagi, A. & Mukohata, Y. Two possible roles of bacteriorhodopsin; a comparative study of strains of *Halobacterium halobium* differing in pigmentation. *Biochem. Biophys. Res. Commun.* **78**, 237-243 (1977).
11. Schobert, B. & Lanyi, J. K. Halorhodopsin is a light-driven chloride pump. *J. Biol. Chem.* **257**, 10306-10313 (1982).
12. Bogomolni, R. A. & Spudich, J. L. Identification of a third rhodopsin-like pigment in phototactic *Halobacterium halobium*. *Proc Natl Acad Sci U S A* **79**, 6250-6254 (1982).
13. Takahashi, T., Mochizuki, Y., Kamo, N. & Kobatake, Y. Evidence that the long-lifetime photointermediate of s-rhodopsin is a receptor for negative phototaxis in *Halobacterium halobium*. *Biochem. Biophys. Res. Commun.* **127**, 99-105 (1985).
14. Braiman, M. & Mathies, R. Resonance Raman spectra of bacteriorhodopsin's primary photoproduct: evidence for a distorted 13-cis retinal chromophore. *Proc Natl Acad Sci U S A* **79**, 403-407 (1982).
15. Gerwert, K., Hess, B., Soppa, J. & Oesterhelt, D. Role of aspartate-96 in proton translocation by bacteriorhodopsin. *Proc Natl Acad Sci U S A* **86**, 4943-4947 (1989).
16. Krautwurst, D., Yau, K. W. & Reed, R. R. Identification of ligands for olfactory receptors by functional expression of a receptor library. *Cell* **95**, 917-926 (1998).
17. Ma, D. & Jan, L. Y. ER transport signals and trafficking of potassium channels and receptors. *Curr. Opin. Neurobiol.* **12**, 287-292 (2002).
18. Nagel, G. et al. Channelrhodopsin-2, a directly light-gated cation-selective membrane channel. *Proc Natl Acad Sci U S A* **100**, 13940-13945 (2003).
19. Bi, A. et al. Ectopic expression of a microbial-type rhodopsin restores visual responses in mice with photoreceptor degeneration. *Neuron* **50**, 23-33 (2006).
20. Schroll, C. et al. Light-induced activation of distinct modulatory neurons triggers appetitive or aversive learning in *Drosophila* larvae. *Curr. Biol.* **16**, 1741-1747 (2006).

Chapter 4

Tetracysteine Motifs on GFP as a Composite Tag

Introduction

Cellular fluorescent protein labeling has been fundamental to the advancement of biological imaging. The use of autofluorescent proteins has enabled noninvasive imaging in living cells and organisms of gene expression, protein trafficking, and other dynamic biochemical signals. Fluorophores have been devised that can directly recognize various components of living cells. Fluorescence techniques using small organic dyes attached by means of antibodies to the protein of interest have long been the foundation of in-vivo imaging despite required cell fixation and permeabilization. Biarsenical dyes are just one type of genetically targeted small organic fluorophore hybrid system that has utility in determination of protein-protein interaction, protein activity, protein function, protein cycling, protein expression with correlative electron-microscopic localization, and rapid in-situ photoinactivation of the genetically targeted proteins. I proposed an imaging technique utilizing a combination of an autofluorescent protein combined with multiple tetracysteines decorating the beta barrel loops complexed into a single tag which, along with a membrane permeable small organic fluorescent dye, combine the advantages of each reporter tool.

Fluorescent proteins

The discovery ¹, gene cloning ², and heterologous expression of the

first fluorescent protein (FP), green fluorescent protein (GFP), from the jellyfish *Aequorea victoria*³ was a revolution in cell biological imaging. Expression of GFP, alone or as a protein fusion, results in visible fluorescence without requiring any cofactors other than O₂. The spontaneous cyclization and oxidation of three amino acids at the core of the 2.5nm by 4.0nm GFP beta barrel form the chromophore. Variations in chromophore covalent structure and the noncovalent environment makes GFP just one member of a growing family of homologous fluorescent proteins of different colors⁴⁻⁶. All references to GFP in this work are referencing the enhanced folding variant Emerald GFP⁷. Laboratory mutagenesis has further diversified the spectra of FPs, increased their brightness and folding efficiencies⁸, and decreased oligomerization⁶. Not surprisingly, given the seemingly impervious FP beta barrel making GFP resilient to their biochemical environment, the FP allows relatively little reactive oxygen species (ROS) to escape upon illumination. Recently, a fluorescent protein, JRED, was mutated and found to liberate ROS, which could photoinactivate fusion proteins⁹. The significant size of FPs means that fusions to FPs may interfere with the localization or function of the protein of interest.

Small Biarsenical Dyes FIAsh and ReAsH

A property of genetically encoded FPs used as markers is that they are fused to the protein of interest so that targeting is precise. Small organic fluorophores for covalent labeling of macromolecules have limited utility in that these dyes lack specificity for any particular protein. Transfection and

transgenic techniques often make exogenous DNA easier than dyes to deliver to cells or organisms. Hybrid systems have been described by which small molecules can be covalently targeted to genetically specified proteins inside or on the surface of living cells, either by spontaneous attachment, enzymatic ligation¹⁰⁻¹² or the tetracysteine biarsenical system¹³,

The tetracysteine biarsenical system requires modification of the target protein by a 12-residue peptide sequence, which includes four cysteines that bind membrane-permeable biarsenical molecules, notably the green and red dyes FIAH and ReAsH¹⁴, with picomolar affinity at which point the dye fluoresces (Fig 4.1a). A small dithiol antidote is co-administered to minimize toxicity and nonspecific binding to endogenous proteins. The tetracysteine motif has undergone multiple rounds of improvement to increase its affinity for the biarsenical dyes enabling lower dye concentrations and allowing for more stringent wash conditions including higher antidote concentrations to reduce nonspecific background staining¹⁵. The tetracysteine-biarsenical complex has shown advantages over FP fusions with tubulin in yeast¹⁶, coupling of receptors to heterotrimeric guanine nucleotide binding proteins (G proteins)¹⁷, translocations to the nucleus¹⁸, and type III secretion of pathogenic proteins from bacteria into eukaryotic cells¹⁹. Tetracysteine-biarsenicals also enable manipulations not readily possible with FPs, such as affinity purification¹⁴, fluorophore assisted light inactivation^{20,21}, co-translational detection of protein synthesis²², pulse-chase labeling^{23, 24} and correlative EM localization²³. Biarsenical dyes are limited in that they have higher background fluorescence

and poorer contrast than FPs, have not yet been demonstrated in intact transgenic animals, require the cysteines to be reduced during labeling and they do not permit two different proteins in the same compartment to be simultaneously labeled with different colors. The tetracysteine sequence occasionally creates a palmitoylation site that can sometimes be mitigated by a preceding epitope tag ¹⁵.

The Tetracysteine (TC) Motif

The earliest designs of the tetracysteine sequences (AEAAAREACCRECCARA) were intended to encourage alpha helicity under the assumption that the biarsenical dye would ideally bind to cysteines across the corresponding positions of each turn of the alpha helix¹³. Though dependent on the level of expression and the specific sequence, with this TC sequence, nonspecific biarsenical background staining was estimated to equal the fluorescence^{14,25}. The background fluorescence can be reduced by increasing the concentration of the dithiols 1,2-ethane-dithiol (EDT) or 2,3-dimercaptopropanol (BAL) in washes to remove the thiol dependent background or by including nonfluorescent dyes to block hydrophobic binding sites²⁶. The amino acids, proline and glycine, were inserted between the dicysteine pairs (AEAAAREACCPGCCARA) to create a hairpin motif with significantly increased the affinity for the biarsenical dye enabling an increase in the tolerable concentration of dithiol competitor without loss of specific fluorescence¹⁴.

The CCPGCC core is the minimum tetracysteine motif necessary for

genetically tagging proteins for staining with biarsenical dyes FIAsh and ReAsH (fig 4.1a). The location in the protein where the TC motif is inserted dramatically affects the ability of biarsenical binding in that the flanking amino acids seem to impact the binding of the ReAsH to the TC motif.

An effort was made to further improve the ReAsH affinity of the TC motif to facilitate more aggressive dithiol washes, hence, further reducing nonspecific background¹⁵. A GFP N terminal peptide library fusion was expressed in HEK293 cells and optimized for ReAsH affinity and GFP-ReAsH FRET in a FACS sorter. This improved ReAsH affinity TC motif (C4) had modified TC core flanking amino acids increasing the motif to the 17 amino acids **GSFLNCCPGCCMEPRSS**. The flanking restriction sites, EcoRI and NotI, correspond to the GS and RSS amino acids of the C4 motif. The C4 motif without the cloning sites is FLNCCPGCCMEP (X4). Neither the C4 nor the X4 motif was transposable. When the TC was appended to the N terminal of GFP, the fluorescent properties of bound ReAsH were altered as compared to when the TC was appended to the C terminal of the GFP. To some degree, the properties could be rescued by the insertion of a 3 amino acid (ESS) flexible linker just prior to the tetracysteine motif (**ESSGSFLNCCPGCCMEPRSS**).

Singlet oxygen

Singlet oxygen ($^1\text{O}_2$) is often prepared by a process called photosensitization. To produce $^1\text{O}_2$, the photosensitizer chromophore is irradiated to its singlet excited state then converted through intersystem

crossing (ISC) to its triplet excited state (the quantum yield of this process is the ISC efficiency or triplet yield) and finally energy is transferred from the triplet state to molecular oxygen. The singlet oxygen production process is usually preferred at low substrate concentration and high oxygen concentration otherwise the excited sensitizer undergo a radical reaction. Singlet oxygen is the lowest excited state of the dioxygen (O_2) molecule. Its lifetime in solution is in the microsecond range. The singlet oxygen quantum yield (Φ_{SO}), or quantum efficiency, is a key property of a photosensitising agent. This quantity is defined as the number of molecules of 1O_2 molecules generated for each photon absorbed by a photosensitizer. Most measurements of Φ_{SO} are made by comparing the unknown to a reference photosensitization standard. Frequently employed photosensitizer standards have values for Φ_{SO} in aqueous media of 0.79 for rose Bengal²⁷. The published values of Φ_{SO} show considerable variations with the solvent, reaction conditions and the measurement technique. Our primary interest with singlet oxygen is that it undergoes several reactions with organic molecules

Chromophore Assisted Light Inactivation (CALI)

CALI is a molecular tool that permits spatial and temporal control in identifying physiological function. In vivo immunolabeling is the most widespread fluorescence technique used to detect endogenous proteins. A primary antibody is used to label the protein followed by amplification with a secondary antibody conjugated to small organic dyes or a phycobiliprotein. Alternatively, primary antibodies can be directly conjugated to fluorophores or

to biotin, which is then detected using fluorophores labeled streptavidin. Direct conjugation is especially useful when injecting antibodies into cells or to increase spectral variety when analyzing multiple proteins. When high-quality antibodies to the target protein are not available, the target can be recombinantly expressed with an epitope tag introducing the complexity of not being completely endogenous. Disadvantages of immunofluorescence are that it is usually restricted to permeabilized cells or extracellular or endocytosed proteins, and the multivalency of these probes might lead to oligomerization of target proteins on live cells. In standard immunolabeling, the size of the fluorophore-targeting complex typically exceeds 200 kD and might interfere with multiprotein recognition in protein complexes.

Flash/ReAsH Chromophore Photosensitizer

Upon binding to a TC motif, both FAsH and ReAsH generate singlet oxygen as well as fluoresce. In live-cell imaging, the fluorophores FAsH and ReAsH also have the ability to photoinactivate proteins to which they are attached. FAsH or ReAsH CALI permits the targeted inactivation of TC tagged recombinant proteins. The exposures required for photoinactivation is on the order of 1000 times the exposure required for fluorescence imaging. The general application of CALI, also referred to as fluorophore-assisted light inactivation (FALI) with fluorescein derivatives, have limited use by lack of mechanistic information regarding target protein sensitivity. Flash FALI was first demonstrated on synaptotagmin I deactivation²⁰. ReAsH CALI has been demonstrated using L-type Calcium channels tagged with N terminal TC²¹.

Current estimates for the range of diffusion of singlet oxygen are 3nm -5nm²⁸⁻
³⁰ though singlet oxygen has been demonstrated to penetrate lipid bilayers as far as 80nm (unpublished results Colette Dooley).

My aim is to show that the degree of CALI possibly could be improved by the presence of multiple chromophores genetically encoded to a targeted protein.

Results and Discussion

Terminal Tetracysteine

The configuration of the TCs on the GFP of the collective biarsenical-GFP reporter is critical in the determining the optical properties of the combined reporter. I initially used the simplest TC, CCPGCC (PG)¹⁴, for binding ReAsH to characterize how the insertion site amino acid environment of the GFP affects the measured fluorescent quantum yield (FQY) of the TC bound ReAsH. The two rigidly spaced arsenics of FIAsh and ReAsH bind with considerable affinity to the dicysteines of PG when the intervening peptides are a proline and a glycine possibly forming a hairpin conformation. The GFP imposes no steric constraints on the bending of the PG hairpin because only one end of the motif was attached to the GFP protein allowing the other end to freely conform to the biarsenical when bound. Depending on which terminal was bound, only one side of the TC had flanking attachment residues. The fluorescent quantum yield of the CCPGCC-ReAsH complex was three times higher when the CCPGCC tag was moved from the C terminal (fluorescent quantum yield ≈ 0.05) to the N terminal (fluorescent quantum yield ≈ 0.16) of

the GFP scaffold (Fig 4.2a), suggesting that the flanking peptides impact the biarsenical dye binding, hence the change in the optical properties. This was an unexpected result because, at the time, the truncation of core tetracysteine flanking residues from peptides was reported to have little effect on the binding and optical properties of the TC-FIAsH complex¹⁴. When considering the secondary structure of the complex, the protein environment adjacent to the N terminal may also impact the binding and spectral properties differently than the protein environment adjacent to the C terminal.

The fluorescent quantum yield of ReAsH molecules bound to a construct with two TCs, CCPGCC, expressed on both ends of GFP (fluorescent quantum yield = 0.05) was comparable to the lower fluorescent quantum yield of the C terminal ReAsH-CCPGCC complex alone. The close proximity of the N and C terminus on the same side of the GFP beta barrel (fig 4.2b), would suggest that the higher N terminal ReAsH-CCPGCC complex fluorescence appeared to be quenched by the presence of the C terminal ReAsH-CCPGCC complex. The scaffold configuration we were using was not an effective way to separate the chromophores. The N and C terminals of GFP extend well beyond the residues that designate the beta barrel (fig 4.2a). To limit the interaction of the N and C terminal ReAsH-CCPGCC complexes, the six amino acids from both termini of GFP were removed without altering the GFP folding and fluorescence³¹ and CCPGCC appended to the truncated termini. The truncated GFP with two terminal ReAsH-CCPGCC complexes had a fluorescent quantum yield that continued to demonstrate quenching

(data not shown). During my observation that the CCPGCC flanking residues impacted the optical character of the ReAsH-CCPGCC complex, Brent Martin evolved an optimized ReAsH binding tetracysteine motif GSFLNCCPGCCMEPGGR, C4¹⁵.

The previous GFP terminal ReAsH-CCPGCC complex quantum yield experiments were repeated using the optimized high ReAsH affinity TC motif, C4 in place of CCPGCC. The N terminal ReAsH-C4 fluorescent quantum yield increased three fold over the N terminal ReAsH-CCPGCC fluorescent quantum yield and was two fold higher than the C terminal ReAsH-C4 fluorescent quantum yield (fig 4.2b). The difference between the N and C terminal fluorescent quantum yields using the C4 motif with identical flanking residues would suggest that the N terminal versus C terminal residue environment had a considerable impact on the binding and optical properties of the ReAsH-TC complex. Comparison of the ReAsH-C4 to the ReAsH-CCPGCC indicated a 4.5 fold increase of the fluorescent quantum yields for the C terminal. It was clear that the flanking residues had a significant impact on the binding and optical properties of the ReAsH-TC complex when attached to a protein. ReAsH chromophores on both terminals of GFP returned a multiple ReAsH-C4 fluorescent quantum yield that equaled to the lower C terminal fluorescent quantum yield alone. Though the overall ReAsH-TC fluorescence increased while using the C4 motif over the CCPGCC, the double chromophore construct quenched the fluorescence to the lower of the

two individual terminal fluorescent quantum yields independent of the TC motif used.

Up to this point, I had assumed but did not measure whether the fluorescent quantum yield was proportional to the singlet oxygen quantum yield. The singlet oxygen quantum yield measured with anthracene dipropionate (ADPA) exhibited a significant 38% drop due to the TC terminal dependence. The N terminal ReAsH-C4 and C terminal ReAsH-C4 singlet oxygen quantum yields were 0.048 and 0.03 respectively. Surprisingly, with a ReAsH-C4 chromophore on both terminals of GFP, a ReAsH-C4 singlet oxygen quantum yield equal to 0.048 was measured, the same optimized singlet oxygen quantum yield as measured on the N terminal alone. This result was encouraging because the double ReAsH-C4 composite GFP tagged protein (ReAsH absorption matched) had half the amount of GFP expression but generated as much singlet oxygen as the single ReAsH-C4 tagged protein suggesting that for a given protein expression, a composite double tagged GFP will produce twice as much singlet oxygen as singly tagged GFP. The disadvantage to this construct with C4 at both termini is that fusion to a protein of interest would unpredictably perturb the adjacent TC.

Tandem TC on GFP N-terminal

To increase the number of ReAsH fluorophores bound to a single GFP and eliminate the variability introduced at the different terminal ends, a tandem series of TCs were appended to the N terminus of GFP. Two, four and eight CCPGCC motifs were strung together on the N terminus of GFP with the

interposed alpha helical linkers EAAAREAAARA¹⁴ (fig 4.3b). With each tandem TC addition, the ReAsH-PG-helix fluorescent quantum yield was lower suggesting that ReAsH quenching was occurring (fig 4.3a). Once again, such quenching presumably indicates that the bound chromophores can come in close contact. Perhaps the linker is too flexible and would be more effective in separating the fluorophore binding sites if it were more rigid.

The assembly of sequential proline residues form a rigid polyproline helix is well-known³². I tried to limit quenching by separating two or four tetracysteines with rigid proline linkers, assembled in tandem on the N terminus of the GFP (fig 4.3b), however, quenching persisted with proline-TC tandem repeats (fig 4.2a). Although the proline helix linker may be rigid, the hairpin conformation of CCPGCC binding sites might position alternating repeat adjacent to each other in a zig zag pattern, allowing for fluorophore quenching.

GFP Loop Insertion Tetracysteine

The GFP protein to which we were appending all the TC constructs is known to be very durable and rigid and could itself serve as a superior scaffold to carry TCs with adequate separation to prevent bound fluorophore quenching. To fully utilize the structure of the GFP to separate two or more tetracysteine bound ReAsH to mitigate fluorophore quenching, the tetracysteines should decorate the GFP on opposite sides or ends of the beta barrel, unlike the fusion to the N and C termini described previously. Therefore I

tried inserting TCs inside the GFP primary sequence, leaving at least one end of the GFP available for fusion to a protein of interest.

Loop insertion sites 156,173,192,212

We chose chose insertion sites before residues 156, 173, 192 and 212 of GFP, because these locations are remote from the termini and were reported to accept peptide inserts while maintaining the fluorescence and structural integrity of the GFP^{33,34}. Insertions at other sites reported to compromise GFP fluorescence and therefore were less attractive. Although GFP fluorescence is not necessary for ReAsH-TC complex formation, the loss of GFP fluorescence would diminish the overall utility of the composite genetic tag, because the GFP would be invisible before labeling and could not be used to pump the ReAsH. Insertion of C4 into all but the 212 location retained GFP fluorescence to some degree. The C4 insertion into position 212 not only extinguished GFP fluorescence but prevented purification with FIAsh beads¹⁴. I presume that misfolding of the GFP created some steric hindrance to the TC binding site and abandoned this location.

Amino acid 173 was found to be the most versatile of the C4 motif insertion sites. At the 173 site ReAsH-C4 had a 0.44 fluorescent quantum yield, nine fold better than 173 ReAsH-CCPGCC (0.05) and almost as good as an optimized N terminus ReAsH-C4 fluorescent quantum yield of 0.48 (fig 4.4a). The 173 ReAsH-CCPGCC fluorescent quantum yield is equal to the C terminal ReAsH-CCPGCC fluorescent quantum yield suggesting that the flanking residues are hindering binding of ReAsH and compromising the

fluorescence. Because the 173-C4 insertion results indicate little change from the optimized C4 characteristics, we were encouraged in that the C4 motif could possibly be a universal TC insertion motif for decorating all insertion locations in the GFP. For cloning purposes, the C4 motif had been optimized with restriction sites BamHI and NotI flanking the three variable amino acids on each side of the core TC, CCPGCC¹⁵. I now removed the flanking restriction sites from the C4 motif to determine if they were a necessary component of the motif. The fluorescence of ReAsH bound to C4 at position 173 and the fluorescence of ReAsH bound to X4 (= truncated C4) at position 173 proved insignificantly different (fig 4.4). Removal of the cloning restriction sites, increased by 20% the quantum yield of singlet oxygen, from 0.048 (C4) to 0.058 (X4), which was also higher than the value for optimized C4 on the N terminal.

Membrane targeting

It was reported that the C4 tetracysteine sequence occasionally becomes palmitoylated^{15,35}, which can sometimes be prevented by a preceding epitope tag¹⁵. I tested the various GFP-TC constructs against the GFP construct with C4 inserted at position 173 to determine if any of the GFP-TC configurations were membrane associated and presumed palmitoylated. The constructs were expressed in HEK293 cells and the cells were lysed by freezing and thawing, after which the membranes were separated from the cytoplasm. The ratio of the membrane fluorescence to the cytoplasm fluorescence (fig 4.5) indicated that the C terminal C4 exhibited low (7%)

membrane association. In some instances a C terminal C4 motif interacts with the membrane particularly when fused to the human cell surface glycoprotein EpCam membrane protein (B.N. Giepmans, personal communication). The PG-helix is the unoptimized tetracysteine, EAAARECCPGCCARA, appended to the N terminal of the GFP. The PG-helix did not seem to get membrane bound (6%) but suffered from low ReAsH binding affinity. The 173-C4 insertion showed 6% membrane association compared to 46% for C4-GFP (C4 on the N terminal of GFP). This is a significant improvement because there is essentially no palmitoylation, the TC is remotely located and therefore unaffected by a fusion protein, yet neither the fluorescent quantum yield nor singlet oxygen quantum yield are significantly compromised as compared to the optimized C4-GFP.

Compromised Loop Insertion Sites 156, 192

Another GFP loop insertion site referenced in the literature, residues 156, had more severe impact on the optical properties of ReAsH-X4. Insertion of X4 at position 156 reduced by 75% both the ReAsH-156-X4 fluorescent quantum yield (0.10) and singlet oxygen quantum yield (0.016) as compared to C4 on the N terminal of GFP (fig 4.4). This unexpected result implied that X4 was not an autonomous universal tetracysteine binding site and that the 156 insertion site would not be a good choice as an insertion site in the genetically encoded multiple tetracysteine GFP tag.

The six flanking amino acids are not the only factors responsible for determining the fluorescent and singlet oxygen properties of ReAsH bound to

a tetracysteine. Tertiary structure must also be considered. Independent of protein folding, the ReAsH should continue to bind the C4 motif if it is not obstructed or the hairpin formation is not hindered. We had demonstrated that fusing the optimized C4 directly to the C terminus dropped the fluorescent quantum yield 40% and the singlet oxygen quantum yield 30% relative to the GFP N terminal C4 fusion. It was reported that the effect of the TC transposition could be mitigated by inserting a floppy linker (ESS) between the GFP C terminal and the C4¹⁵. The fluorescent quantum yield recovered to 0.46 from 0.25 though the singlet oxygen quantum yield only rebounded slightly to 0.03 from 0.026. To reduce insertion stresses on the TC, I thought it would be worthwhile to try to flank the 156-X4 insertion with a floppy linker to try and recover some of the optimized ReAsH-X4 fluorescence and singlet oxygen production as measured with C4 on the N terminal. Perhaps due to residue environment or steric constraints of the insertion site, inclusion of the floppy linkers flanking the X4 insertion does not restore the X4 ReAsH properties to the optimal values (fig 4.6).

The last attempted referenced receptive insertion site is in the last loop of GFP before residue 192. The insertion of X4 into position 192 considerably reduced GFP fluorescence, but the TC construct bound FIAsH beads and was able to be purified. The 192 site minimally impacts the optimized properties of the X4 tetracysteine and returns a ReAsH-192X4 fluorescent quantum yield of 0.40 though the singlet oxygen quantum yield was reduced to 0.0184, just 37% of the optimal value. The 192 construct posed a conundrum in that the

ReAsH singlet oxygen and GFP quantum yields were dramatically compromised whereas ReAsH fluorescence remained high.

Many different constructs containing various tetracysteine motifs and insertion sites had been evaluated for their fluorescence and singlet oxygen generation capabilities. The absolute conditions that control both the bound ReAsH fluorescence and singlet oxygen generation are not clear, but they are roughly proportional (fig 4.7). If fluorescence and intersystem crossing were dominant mechanisms to deactivate the excited state, their quantum yield should sum to 1 and increases in one would be at the expense of the other. Instead, both quantum yields are much less than 1 so both can improve in parallel if competing quenching mechanisms are reduced. The binding conditions that control the generation of singlet oxygen remain largely empirical. The issue is raised regarding the methodology of evaluating the receptive insertion points. Evaluating TCs individually inserted into GFP may be flawed because a change imposed by one insertion might be compensated by another insertion in another loop.

GFP with Multiple Tetracysteine Insertions

We have already considered terminal double tetracysteine constructs and tandem multiple tetracysteine constructs and found that the fluorescence was quenched most likely due to the close proximity of the tetracysteines, hence the ReAsH fluorophore, to each other. The 212 insertion site construct resulted in C4 losing its ability to bind ReAsH and was no longer considered viable for constructing a multiple TC decorated GFP tag. The remaining sites

were paired with the 173 insertion site, which retained a reasonable fluorescent quantum yield and singlet oxygen quantum yield. Both 156 and 192 were on the opposite side of the beta barrel from 173 and therefore were good candidates to avoid proximity quenching with the 173 insertion. A composite tag with X4 at the 156 and 192 site was not attempted because both these sites are on the same side of the GFP beta barrel and was thought to result in ReAsH quenching similar to what was observed when TC-ReAsH complexes were on both the N and C termini.

156X4 and 173X4 insertion

The fluorescent quantum yield of ReAsH bound to the multiple X4 motifs on GFP just before residues 156 and 173 was approximately the average of the quantum yield values of ReAsH bound to each site individually as was the case with the singlet oxygen quantum yield (fig 4.6), as would be expected from non-interaction chromophores. Therefore, it would be advantageous to try to increase the lesser of the quantum yields to increase the overall average.

173-X4 and 192-X4 insertion

Insertion of X4 before amino acids 173 and 192 on a single GFP scaffold resulted in a fluorescent GFP that bound two ReAsH molecules and retained a high fluorescent quantum yield of 0.4 and a singlet oxygen quantum yield of 0.036. The fluorescence of the GFP was reduced to 0.16 from 0.6 as was the case with the 193-X4 construct alone, but the poor folding or chromophore interference does not seem to compromise the ReAsH

properties. The 173-192-X4 construct was the most promising of all the wholly internal insertions tested. All the tetracysteines were isolated from the GFP terminal ends which allowed for autonomous protein fusions. Transfection into mammalian cells indicated that membrane targeting of the construct was not observed while maintaining a sufficient ReAsH fluorescent and singlet oxygen quantum yield.

C4-GFP173-X4 insertion

The construct with an optimized tetracysteine on the N terminal and inserted before residue 173 of GFP (C4GFP173C4) is the construct with the highest double TC singlet oxygen quantum yield (0.036) while retaining a reasonable fluorescent quantum yield (0.33). Connexin43 (**Cx43**), a gap junction protein, has been shown in the laboratory to tolerate a C terminal optimized TC without compromising the biarsenical binding or gap junction function. Dr. Thomas Deerinck cloned the C4GFP174X4 double TC-GFP composite tag onto the C terminal of Cx43 and transfected HEK293 cells. His initial observations indicated that the double TC-GFP tag has a ReAsH:GFP ratio that is 2.5 times greater than the single TC-GFP composite tag ReAsH:GFP ratio on Cx43 (fig 4.8).

Only the in-vitro measurement of singlet oxygen was performed for the different constructs. It is expected from the measured singlet oxygen quantum yields that the C4GFP173X4 tag would be 1.5 times more effective in CALI than the 173X4 composite tag. The generated singlet oxygen quantum yield is commonly accepted to have a direct relation to the degree of photoinactivation

possible to the fusion protein. This photoinactivation or chromophore-assisted light inactivation (CALI) permits the targeted inactivation of tagged proteins and offers important advantages such as spatial and temporal control in identifying physiological function. Though no CALI quantization was performed with any of the construct in-vivo, the ability to do photoconversion was tried with the 173X4 construct with Cx43. Thomas Deerinck expressed the 173X4 fused to the C terminal of Cx43. The cells were labeled with ReAsH. In the presence of DAB, the ReAsH was excited. The composite tag labeled gap junctions had produced enough singlet oxygen to polymerize the DAB and the gap junctions were clearly visible (fig 4.9).

Materials and Methods

Tandem TC with Helix linker Constructs

The tandem TC constructs were generated by annealing the 5' phosphorylated TC oligo GATCCGCCGAGGCCGCGCCCGCGAGGCCTGCTGCCCAGGCTGCGCCCGCGCCA and its complement oligo GATCTGGCGCGGGCGCAGCAGCCTGGGCAGCAGGCCTCGCGGGCGGCCTCGGCG producing sticky BamHI and BglII sites on 5' and 3' ends respectively of the TC double stranded DNA fragment. The annealed TC fragments were ligated together creating a tandem repeat assembly with TC sets oriented in forward and reverse direction. The ligation was purified with a gel purification column (Qiagen) and digested with BamHI and BglII restriction enzymes. The digestion was run on a 1% agarose gel and a ladder of tandem repeat TCs

was produced. The ligation of BamHI to BglII creates a linker that was neither cut by BamHI nor BglII so that only reverse orientation TC homoligations were digested by BamHI and BglII. Each component of the TC ladder represented a different number of TC tandem repeats. The tandem repeat bands were purified from the gel and then subcloned into pRSETB vector with a GFP emerald construct containing an N terminal digested and dephosphorylated BglII site after the ATG start codon. The DNA was amplified by transforming DH5a *E. coli* and then grown in LB media with ampicillin antibiotic. The DNA was purified from the *E. coli* using miniprep DNA purification column (Qiagen) and sequenced to verify the number of repeats and the TC repeat orientation.

Tandem TC with Proline linker Constructs

A TC with a five proline linker was appended via a BglII linker to the N terminus of emerald GFP using the forward nested primers GGCTGCTGCC CTCCTAGATCTATGGTGAGCAAGGGCGAG and GGATCCCCTCCTCCTCC TTGCTGCCCCGGCTGCTGCCCTCCTAGATCT and the reverse primer GCGCGAATTCTTACTTGTACAGCTCGTCC. The PCR fragment was digested with BamHI and EcoRI then subcloned into the BamHI and EcoRI sites of pRSETb bacterial expression vector then amplified by transforming into DH5a bacterial cells and DNA purified. The resulting vector was digested with BglII and EcoRI and the PCR fragment was ligated into the receptive subclone vector digested with BamHI and EcoRI to generate a double TC separated by 5 prolines. The double proline TC construct was digested with BglII and EcoRI and the PCR fragment was ligated into the receptive vector to

generate a triple TC with 5 proline linkers. This iteration process was repeated until eight proline tandem TC repeats were added to the N terminus of emerald GFP.

173-C4 Construct

The phosphorylated RNA initiated overhang cloning oligonucleotide primer CCAGGcTGCTGCATGGAGCCGGACGGCAGCGTGCAGCTCGCC GACCACTA and the complement GCCTGgGCAGCAATTCAAAAACCTCGAT GTTGTGG CGGGTCTTGAAGTTCACCTTGATGCCGT (Uppercase denotes Deoxyribonucleotides and lower case denotes ribonucleotides) were used to generate Emerald GFP PCR products of the complete pBAD (Invitrogen) Emerald GFP template vector around the C4 tetracysteine motif insertion between amino acids 172 and 173. The GFP PCR product was ligated overnight at 16C then transformed into LMG E. coli bacterial cells and plated on LB amp plates. A single colony was picked and grown in 50ml LB amp media where the emerald GFP construct is expressed and purified.

156-C4 Construct

The 156-C4 construct was assembled in a similar manner to that of the 173-C4 construct. The 156-C4 construct was assembled using the phosphorylated RNA initiated overhang oligonucleotide primers CCCGGgTGC TGCATGGAGCCGCAGAAGAACGGCATCAAGGTG and the complement CCCGGgGCAGCAATTCAAAAACCTTGTCGGCGGTGATATAGAC. These primers specify the insert location of the C4 between the 155 and 156 amino acid of emerald GFP.

The 156-C4 insertion construct was modified with three amino acid GSS flexible flanking linkers. Two Emerald GFP PCR fragments around the 156 insertion site were produced using nested PCR forward primers ATGGAGCCGGGCAGCAGCCAGAAGAACGGCATCAAGGTG and GCCCCGGGTGCTGCATGGAGCCGGGCAGCAGC with the emerald reverse primer GCGCGAATTCTTACTTGTACAGCTCGTCCATGCC and nested reverse primers GCAATTCAAAAAGCTGCTGCCCTTGTCGGCGGTGATATAGAC and CACCCGGGGCAGCAATTCAAAAAGCTGCTGCC with the emerald GFP forward primer GCGCCATATGGTGAGCAAGGGCGAG. The PCR fragments encoded an N terminal emerald GFP fragment with an NDE site just prior to the ATG start codon followed by emerald coding sequence up to the sequence coding for amino acid 155 at which point the nucleotides coding for GSS amino acids are inserted before the FLN amino acids of the X4 motif ending with XMN restriction site which corresponds to the PG amino acids of the C4 motif. The second PCR fragment is the C terminal portion of emerald GFP initiated with the XMN restriction site of the PG amino acids of C4 followed by the MAPGSS and the remainder of emerald GFP terminated with an ECORI site after the TAA termination codon. The PCR fragments are both digested with XMN and ligated together at 16°C overnight. The ligation product is run on a 1% agarose gel where three ligation products are observed. The 730 base pair ligation product, corresponding to full length emerald GFP, is excised and gel purified and digested with NdeI and EcoRI restriction enzymes. This digestion is purified and subcloned into the NdeI and

EcoRI sites of the pBAD bacterial expression vector where the construct expression was initiated with arabinose in the LMG E coli cell line .

193-C4 Construct

The 193-C4 construct was assembled in a similar manner to that of the 173-C4 construct but the 193 construct used the phosphorylated RNA initiated overhang oligonucleotide primers CCCGGmGTGCTGCATGGAGCCGGTGCTGCTGCCCCGACAACCAC and the complement CCCGGmGGCAGCAATTCAA AAAGGGGCCGTCGCCGATGGGGGT. These primers insert the C4 between the 192 and 193 amino acid of emerald GFP.

Protein Purification and Fluorescence Measurements

Bacterial cells expressing the construct to be tested were lysed in B-PER buffer (Pierce) supplemented with 10 μ M sodium 2-mercaptoethanesulfonate, MES(Sigma), 1 μ M tris-(2-carboxyethyl) phosphine HCL, TCEP (Molecular Probes) and complete protease inhibitor (Roche). All subsequent solutions contained 10 μ M MES and 1 μ M TCEP. The cellular debris was pelleted and the soluble cell lysate was combined with prewashed FIAsh beads¹⁴ and incubated for 1 hour at 4°C after which the beads were pelleted and washed three times in PBS and once in PBS supplemented with 0.1 mM EDT. The protein was eluted with 0.25 M dithiothreitol, DTT (Invitrogen). The elution was buffer exchanged in PBS four times by centrifugation in a 30 kDa-cutoff Microcon filter (Millipore). Protein was labeled with 3 fold excess ReAsH biarsenical for 1 hour at room temperature then buffer exchanged four times in PBS followed by one wash in PBS with 0.1 mM

BAL to remove free ReAsH. ReAsH-TC combination quantum yields were determined using rhodamine 101 in ethanol ($n = 1.0$) as a standard then corrected for refractive index discrepancy between ethanol and water.

Determination of Singlet oxygen quantum yield (Φ_{so})

Singlet oxygen quantum yields were determined using the relationship

$$\text{SOQY} = \text{SOQY}_{\text{RB}} \frac{K_{\text{S}}}{I_{\text{S}}} \frac{I_{\text{RB}}}{K_{\text{RB}}}$$

where K_{S} and K_{RB} are respectively observed rate constants for loss of anthracene dipropionate from the sample and rose bengal standard. I_{S} and I_{RB} are respectively rates of photon absorption capture by the sample and rose bengal standard. SOQY_{RB} was the reported rose bengal standard singlet oxygen quantum yield.

The TC decorated GFP constructs in pBAD bacterial expression vectors were transformed into LMG E coli and plated on ampicillin selective media, and incubated overnight at 37°C. One colony was picked and grown in a 250ml Erlenmeyer flask with 50ml of LB supplemented with 50 μM ampicillin for 8 hours until the OD_{600} was approximately 0.4 at which point an additional 100mL-50 μM ampicillin SOB supplemented with 2% arabinose was added to the flask to induce protein expression bringing the total volume to 150mL which reduced the total media surface area in the flask and effectively

restricted the growth conditions of the bacteria. The arabinose induced bacteria grew overnight at which point the bacteria was pelleted and divided into aliquots of 200ul of bacteria and frozen at -80°C . An aliquot was thawed and B-Per lysed and purified over flash beads and stained with ReAsH. ReAsH stained purified protein with a ReAsH absorption of 0.05 was combined with 50 μM anthracene dipropionate (ADPA) to a total volume of 80ul and placed in a quartz microcuvette. The ADPA absorption spectrum was recorded from 350nm to 700nm. The ReAsH was excited with a xenon arc lamp through a 590/45nm bandpass filter resulting in an excitation power concentration of 0.7 watts/cm². The excitation power concentration was normalized to the excitation power spectrum of the xenon lamp spectrum imposed on the bandpass filter. The ReAsH excitation power spectrum was convolved with the individual ReAsH-TC bound construct or rose Bengal standard absorption spectrum to determine the total energy absorbed by the fluorophore. The ADPA absorption was sampled after every 5 minutes of exposure until the ADPA absorption at 380nm (abs_{380}) was half the original value. The natural logarithm of ADPA abs_{380} was plotted against exposure time and the extinction decay slope determined. The energy absorbed by the fluorophore was determined by correlating the absorption spectrum with the excitation spectrum from the filter and lamp for both the sample and the rose bengal standard according to the equations.

$$I_{\text{ABS}} = I_0(\lambda) - I_{\text{TRANS}}(\lambda)$$

$$I_{\text{ABS}} = I_0(\lambda) [1 - 10^{-\epsilon(\lambda)CL}]$$

$$I_{\text{ABS}} = I_0(\lambda) [1 - 10^{-\text{ABS}(\lambda)}]$$

$$\epsilon_{\text{ABS}} = I_0(\lambda) [1 - 10^{-\text{ABS}(\lambda)}]$$

I_{ABS} = Intensity absorbed
 $I_0(\lambda)$ = Incident intensity
 $I_{\text{TRANS}}(\lambda)$ = Transmitted intensity
 $\epsilon(\lambda)$ = extinction coefficient
 C = speed of light
 L = path length

Singlet oxygen quantum yields were determined using rose bengal in methanol ($\phi_{\text{SO}} = 0.75$) as a standard then corrected for refractive index of methanol relative to water by a factor of 0.96.

Conclusion

The kinetics and functional biology of protein trafficking have been greatly advanced through live cell imaging using genetically encoded reporter protein fusions with GFP. The small 6 to 20 amino acid tetracysteine motif paired with a membrane permeable biarsenical ligand allows to live cell imaging, CALI and photoconversion. To combine the features of both systems, I proposed a protein labeling tool comprised of a tetracysteine decorated GFP hybrid reporter that uses the rigid beta barrel structure of the GFP to separate bound ReAsH fluorophores to prevent close proximity fluorophore quenching. This TC-GFP hybrid reporter was developed to increase the number of ReAsH fluorophores labeling each fusion protein hence amplifying the effective fluorescence and singlet oxygen generated per protein.

I compared quantum yields for ReAsH fluorescence and ReAsH singlet oxygen production of TC-GFP constructs bearing one or more tetracysteine sequences in various locations on the beta barrel. The quantum yields depended on the insertion site and its amino acid environment. To reduce such dependency, I tested a longer TC motif, C4, GSFLNCCPGCCMEPRSS recently evolved in the laboratory. The high affinity motif, introduced at various positions on the GFP structure, produced fluorescent quantum yields and singlet oxygen quantum yields that were still sensitive to insertion location, suggesting that the invariant flanking amino acids do not insulate the tetracysteine motif from its structural context. Inserting a flexible linker before the GFP C terminal C4 restored the optimized C4 properties. The insertion of the optimized motif into position 153 severely compromised the ReAsH properties of this construct. Flexible linkers flanking the C4 insertion at position 153 of GFP did not have the same restorative effect as at the C terminus. The N terminal TC consistently has a significantly higher fluorescent quantum yield. This was not surprising for the ReAsH-C4 complex because the C4 motif was optimized on the N terminus. It could be fruitful to optimize the TC on the C terminal to try and improve the C terminal characteristics. The only insertion site in GFP that readily receives the C4 motif and retains the ReAsH character of the optimized motif and the fluorescent character of the GFP is between the 172 and 173 residues of GFP.

The C4 TC motif fused to a protein often provides a palmitoylation site that directs the expression to the plasma membrane. With the CCPGCC core

flanked by the helix linkers, there is no palmitoylation though there is a compromise of bound ReAsH fluorescence intensity. The insertion of C4 TC into the 173 site of GFP retains the high ReAsH binding, fluorescent and singlet oxygen production characteristics of the optimized C4 but avoids palmitoylation.

Expression and ReAsH labeling of membrane proteins can be compromised by the fusion to C4. The optimized performance of the C4 tag could be exploited with membrane proteins by fusing a 173-C4 composite tag. Because the 173-C4 insert position on the opposite side of the beta barrel perhaps makes the C4 motif less susceptible to interaction with the membrane allowing for the ReAsH binding as opposed to the C4 on the terminal end of the of the fusion protein where it is able to interact with the membrane.

The double chromophore construct with an N terminal C4 and a 173 C4 was found to be a viable genetically encoded multi TC tag but suffered from the complications of the N terminal C4 construct and therefore had limited utility. Multiple tetracysteine constructs tested with insertion of X4 in positions 173 and 192 of emerald GFP provided a composite tag without a terminal C4 and the associated complications. The GFP fluorescence was somewhat compromised and could perhaps be recovered by using a superfolder version of GFP but there is very little ReAsH fluorescence quenching and the singlet oxygen production remain efficient.

The relationship between the TC motif, secondary structure environment, and the quantum yield proved to be very complicated and

marginally understandable. Considering all the constructs tested, there was a general positive correlation between the fluorescent quantum yield to singlet oxygen quantum yield.

The effective fluorescent quantum yield and singlet oxygen quantum yield of multiple chromophores on a single GFP scaffold was approximately the average of the individual ReAsH chromophore quantum yields for ReAsH single site insertions. To increase the average QY of a multi TC-GFP tag, it would make sense to improve the quantum yield of the ReAsH at the individual sites. I attempted directed random mutagenesis of the tetracysteine sequence in various receptive sites on the GFP and proposed to screen for singlet oxygen production by reacting biotin hydrazide with singlet-oxygen-damaged histidines. Phage display of GFP with a tetracysteine library inserted before residue 173 was to be screened for binding affinity and singlet oxygen production. Preliminary experiments with bacterial display and biotin hydrazide indicated that singlet oxygen sorting is possible though bacterial display has experimental limitations for the library size. I attempted phage display of a GFP library but it was challenging because the large GFP protein was not stably displayed on the surface of T7 phage.

Further possible modifications to the tetracysteine decorated FP would be to create a construct on CFP to bind with FIAsH. The insertion of the C4 motif into the individual loop amino acid environment affects the properties of the C4. The 173 GFP insertion site residues are identical to the insertion site

residues of CFP but small changes in the secondary structural environment can have a large impact on the function of the biarsenical optical properties.

Though here we have only used the GFP as a rigid scaffold, the GFP could function as an antenna for pumping the ReAsH chromophore (Gaietta G, PNAS in press) and increase the signal to noise ratio of the labeled protein. By only pumping the ReAsH bound to GFP and not the cellular nonspecific bound ReAsH the background ReAsH fluorescence should be reduced.

Some initial singlet oxygen quantum yield measurements of 173 C4 indicated that the 173-C4 insertion itself generated singlet oxygen without bound ReAsH. The mechanism is not clear but we propose that the insertion at 173 compromises the beta barrel chromophore shielding and allows entry of O₂ and escape of the singlet oxygen generated from the core chromophore. Initial in-vitro experiments indicated that the amount of singlet oxygen generated was 25% of the singlet oxygen generated from ReAsH. GFP mutagenesis and singlet oxygen screening are necessary to improve the singlet oxygen generation capabilities of this construct. This is an exciting result because it would provide a genetically encoded singlet oxygen generator independent of synthetic ligands such as ReAsH. Another FP, killer red, has been speculated to generate singlet oxygen⁹ but, initial tests with anthracene dipropionate indicate that singlet oxygen production is undetectable, i.e. QY<0.0025. Therefore Killer Red is unlikely to photoconvert DAB, and the ROS effects observed are due to species other than singlet oxygen.

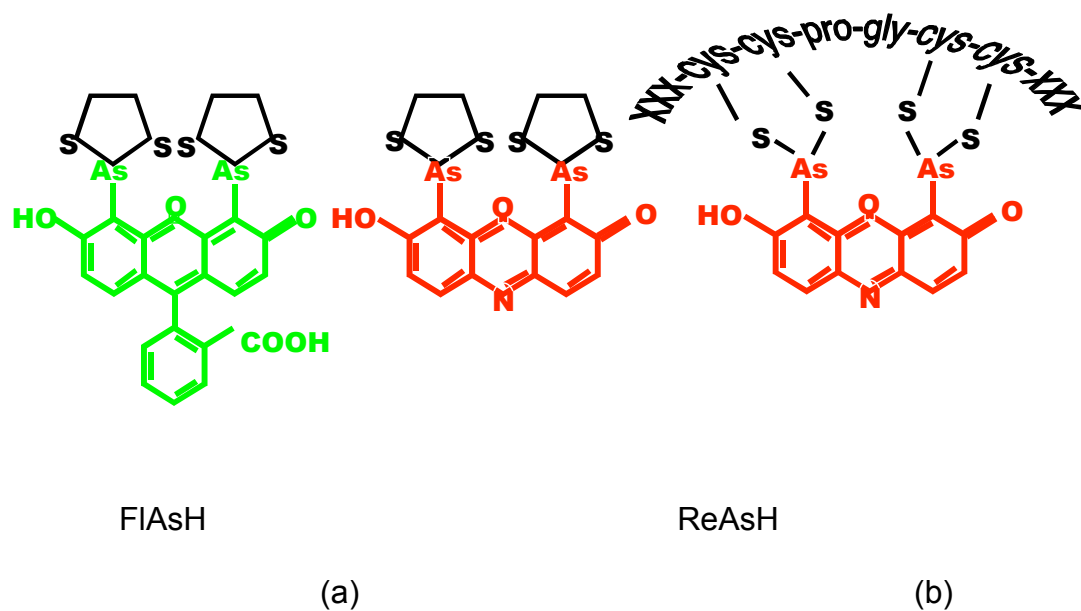


Figure 4.1 FIAsH and ReAsH small molecules and binding configuration. (a) FIAsH and ReAsH small molecule with EDT dithiol antidote bound to the arsenics (b) proposed binding conformation of ReAsH bound to core tetracysteine hairpin¹⁴.

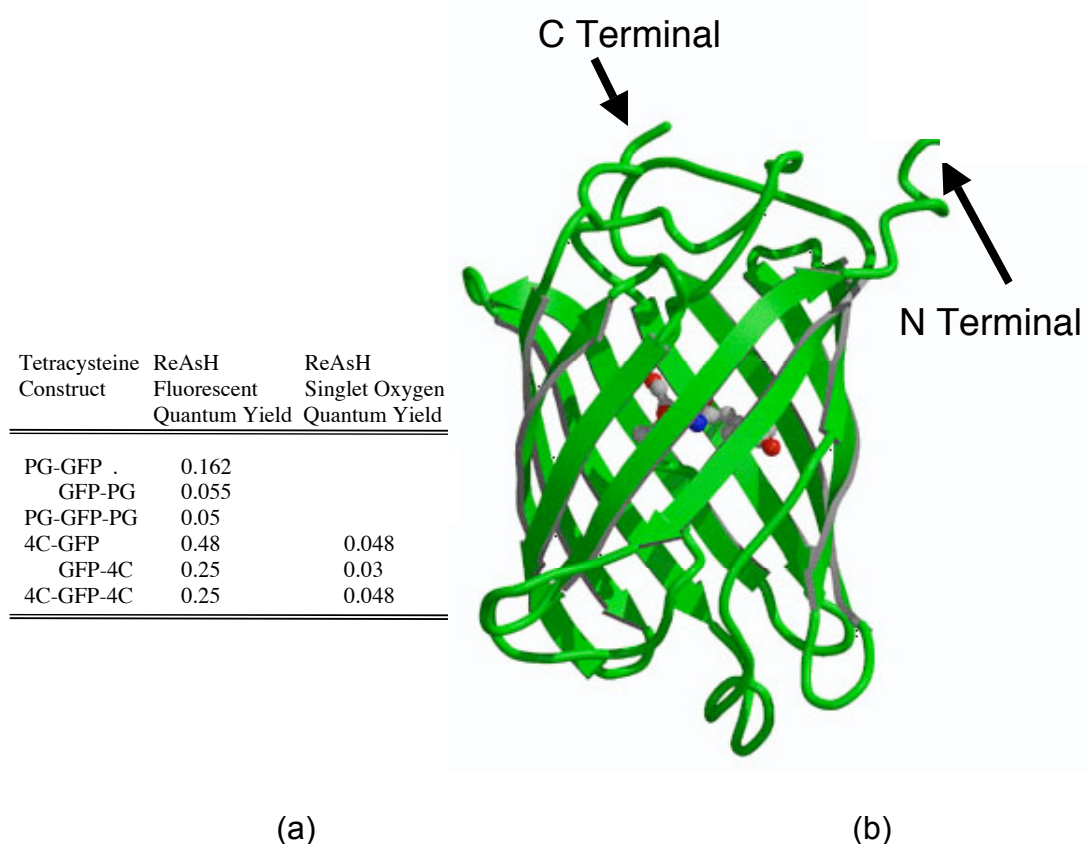


Figure 4.2 GFP-TC configuration and ReAsH quantum yields. (a) Measured ReAsH Quantum yield of various single and multiple TC constructs. PG tetracysteine is simply the minimum motif ,CCPGCC , with out flanking residues. Quantum yield measurements were performed with the tetracysteine attached to the N terminal of emerald GFP meaning that there are no N terminal flanking amino acids aside from the initial methionine and the first residues of the GFP are the other flanking residues. Samples with ---- indication were not tested. (b) Cartoon representation of GFP molecule showing close proximity of the GFP N and C termini and the long terminal residues.

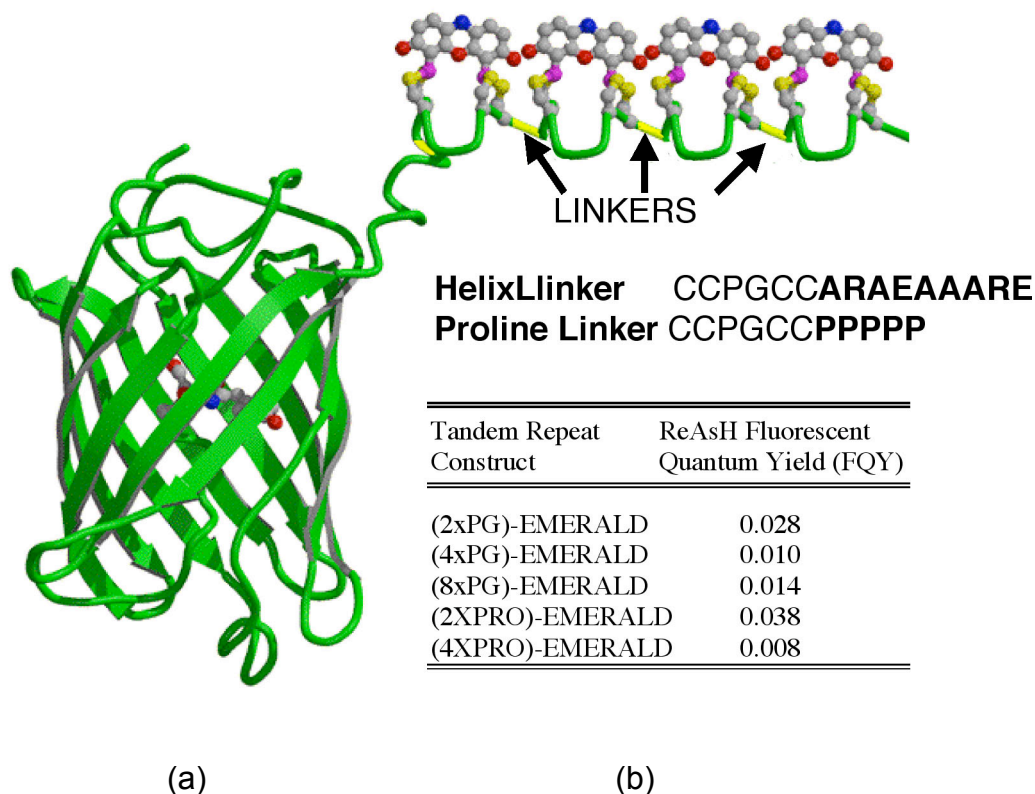
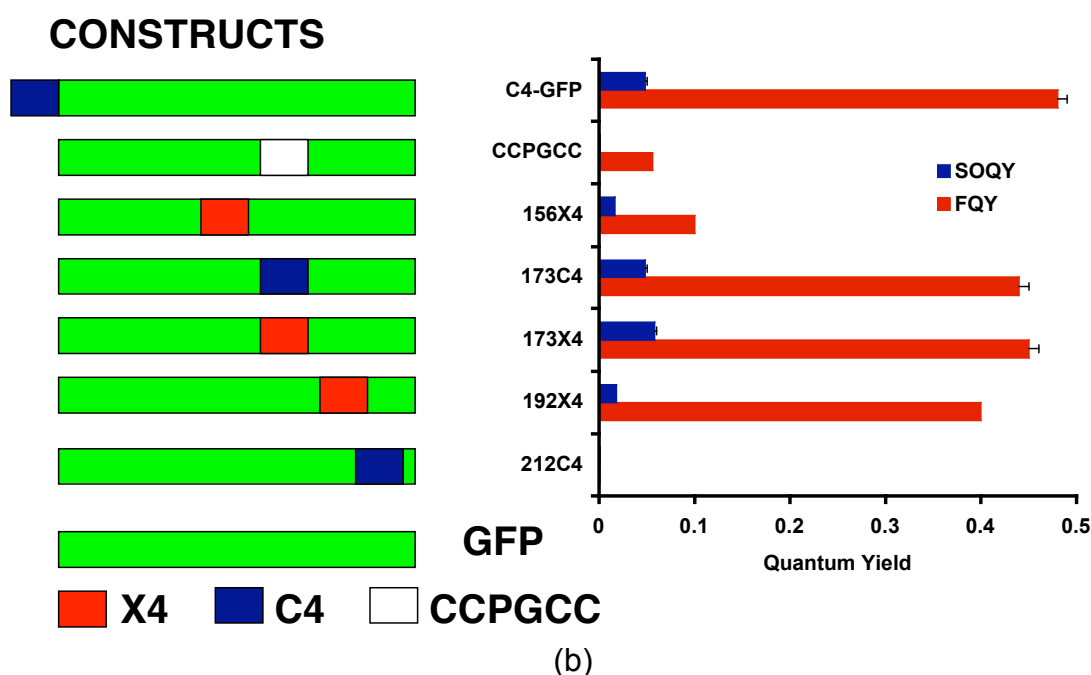


Figure 4.3 Tandem TC constructs and ReAsH quantum yields. (a) All tandem repeat assemblies are displayed on the N terminal of GFP. Constructs with helix flexible linkers, EAAARECCPGCCARA, and five proline rigid linkers, PPCCPGCCPPP, were ReAsH absorption matched and the fluorescent quantum yield measured and compared to a known fluorescent standard (rhodamine 101). (b) All Tandem tetracysteine constructs demonstrated fluorophore fluorescent quenching regardless of linker. None of the optimized tetracysteine linkers were tested in tandem here though tests in-vivo indicated that there is quenching as well with the optimized motif.

Tetracysteine Construct	ReAsH Fluorescent Quantum Yield (FQY)	ReAsH Singlet Oxygen Quantum Yield (SOQY)
CCPGCC	0.056	
156X4	0.10	0.016
173C4	0.44	0.048
173X4	0.45	0.058
192X4	0.40	0.018
212C4		

(a)



(b)

Figure 4.4 TC GFP insertion quantum yields. Tetracysteine insertions before amino acids 173, 156, 192 and 212 of emerald GFP. C4 is the complete optimized TC with cloning restriction sites, GSFLNCCPGCCMEPGGR. X4 is the optimized TC without cloning restriction sites, FLNCCPGCCMEP. The core TC CCPGCC insertion into site 173 shows severely compromised quantum yields. X4 insertion demonstrates a marginal improvement in ReAsH fluorescent quantum yield but shows a marked improvement in ReAsH singlet oxygen quantum yield. The singlet oxygen quantum yield of 192 and 156 are both relatively low and both are on the same side of the emerald GFP beta barrel. Construct 212C4 did not bind ReAsH

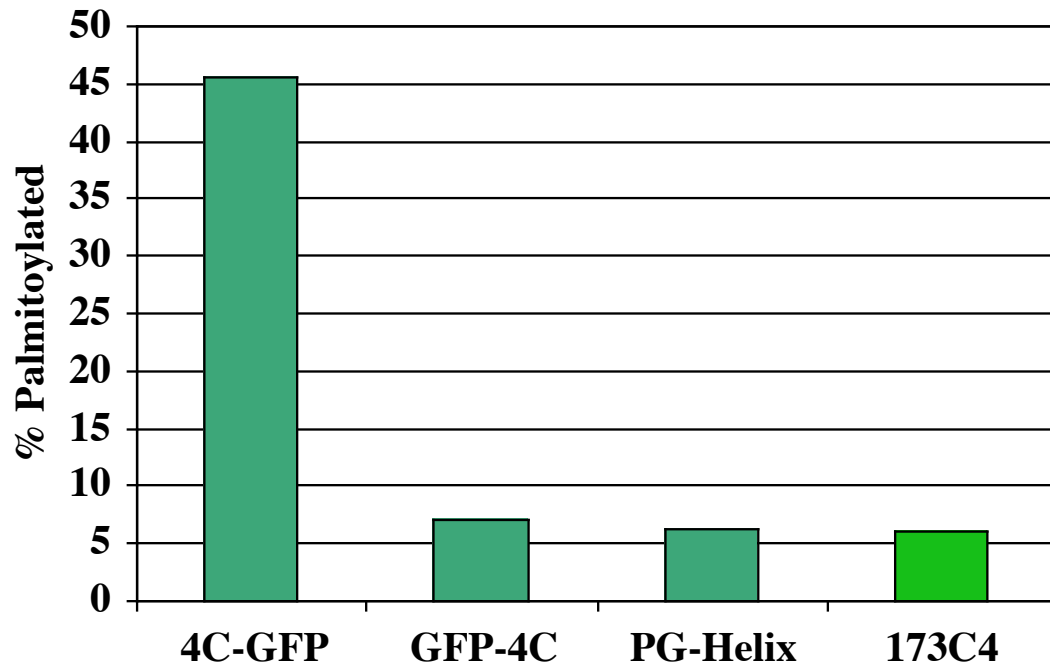
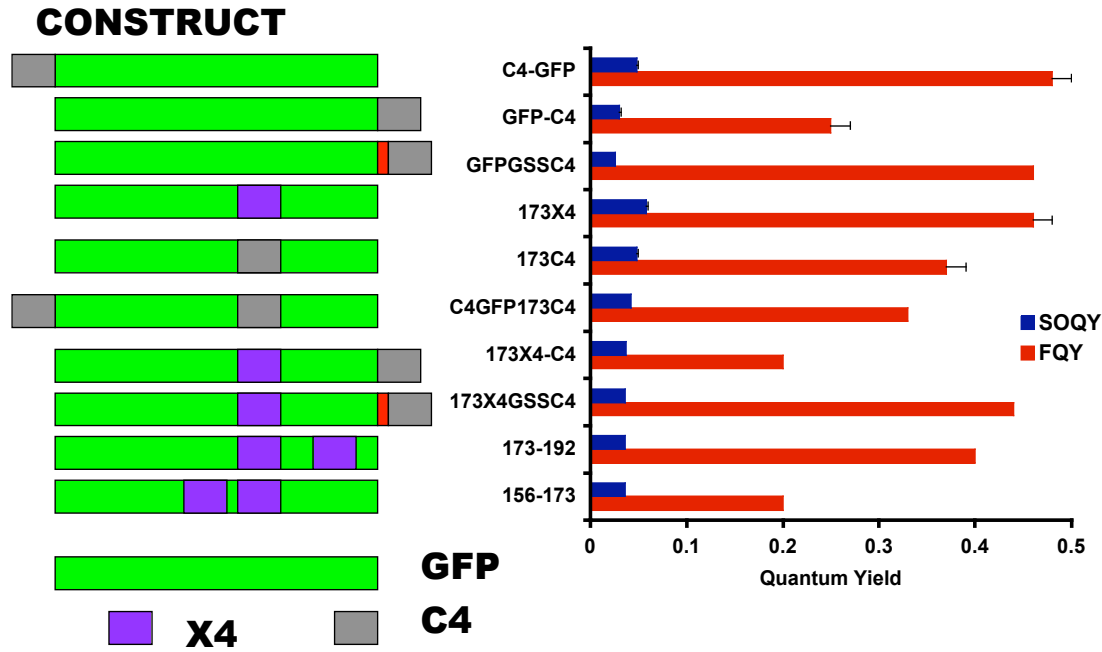


Figure 4.5 Membrane association of TC tagged GFP constructs. C4 fused to the N terminus of GFP (C4-GFP), C4 fused to the C terminus of GFP (GFP_C4), PG with a helix linker AEAAARECCPGCCARA fused to the N terminus of GFP (PG-GFP), and C4 inserted before residue 173 of GFP (173C4). 173C4 demonstrated the least amount of membrane association and does not have the tetracysteine terminal effects experienced with the other constructs.

Tetracysteine Construct	Fluorescent Quantum Yield	Singlet Oxygen Quantum Yield	ReAsH Fluorescent Quantum Yield	ReAsH Singlet Oxygen Quantum Yield
GFP-C4	0.68	0.0	0.25	0.030
GFPESSC4	0.68		0.46	0.026
GFP173X4	0.60	0.010	0.46	0.058
GFP173C4	0.58	0.010	0.37	0.048
C4-GFP173X4	0.58		0.33	0.042
GFP173X4-C4	0.58		0.20	0.037
GFP173X4ESSC4	0.58		0.44	0.036
GFP 173 192	0.15		0.40	0.036
GFP 156 173	0.40		0.20	0.036

(a)



(b)

Figure 4.6 Multiple TC tagged GFP quantum yields. (a) Fluorescent quantum yield and singlet oxygen quantum yield Measurements for GFP and ReAsH of Multiple TC constructs decorating a GFP Scaffold (b) constructs pictorial and bar graph of FQY vs SOQY

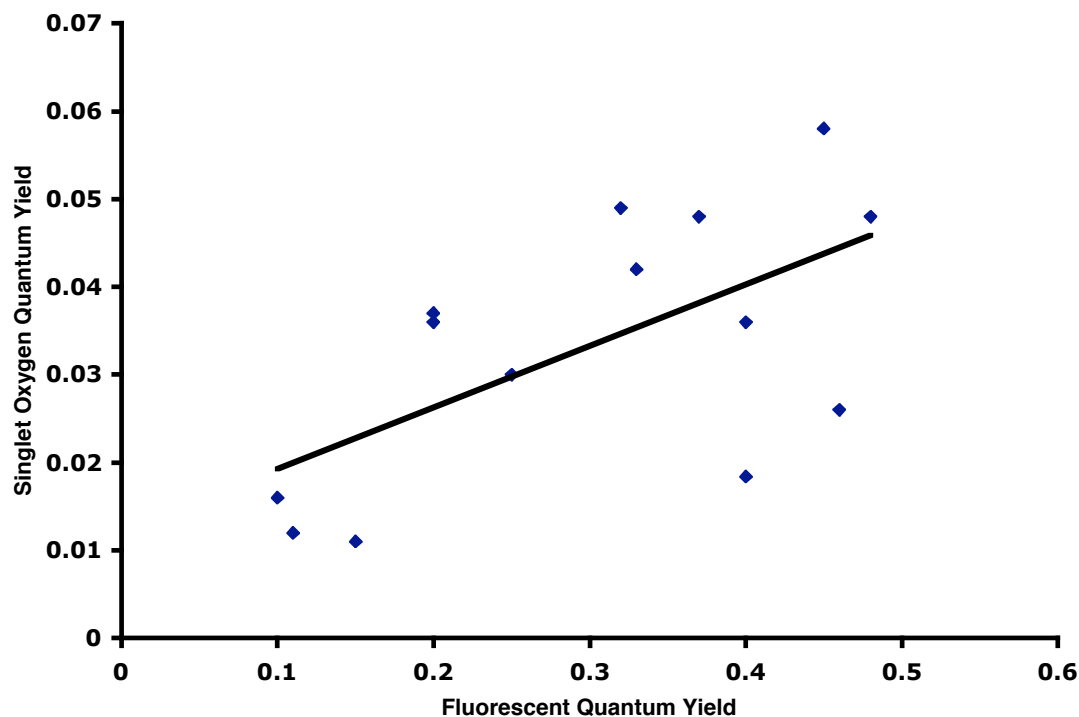


Figure 4.7 Singlet oxygen vs. fluorescent quantum yields. At quantum yields much less than 1.0, the relationship of ReAsH fluorescent quantum yield to singlet oxygen quantum yield is generally positively correlated, higher fluorescent quantum yield corresponds to a higher measured singlet oxygen quantum yield. It would be expected that at higher quantum yields near 1.0, the relationship would be inversely correlated.

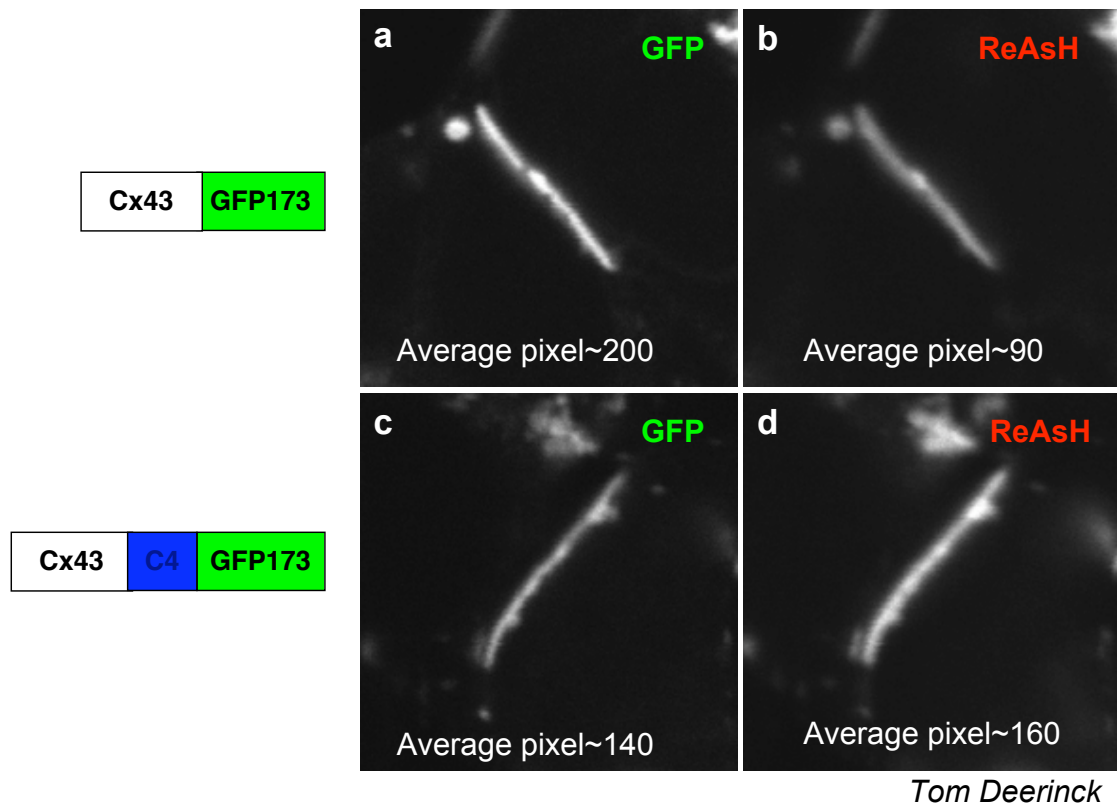


Figure 4.8 Relative Fluorescence of Cx43-GFP173 (a) Cx43 with a C terminal GFP173 composite tag with ReAsH has an average GFP fluorescent pixel intensity value of 200. (b) Same tagged connexin43 gap junction as in image (a) stained with ReAsH has an average ReAsH fluorescent pixel intensity value of 90 (c) Cx43 with a double TC C terminal C4-GFP173 composite tag with ReAsH has an average GFP fluorescent pixel intensity value of 140. (b) Same tagged connexin43 gap junction as in image (c) stained with ReAsH has an average ReAsH fluorescent pixel intensity value of 160

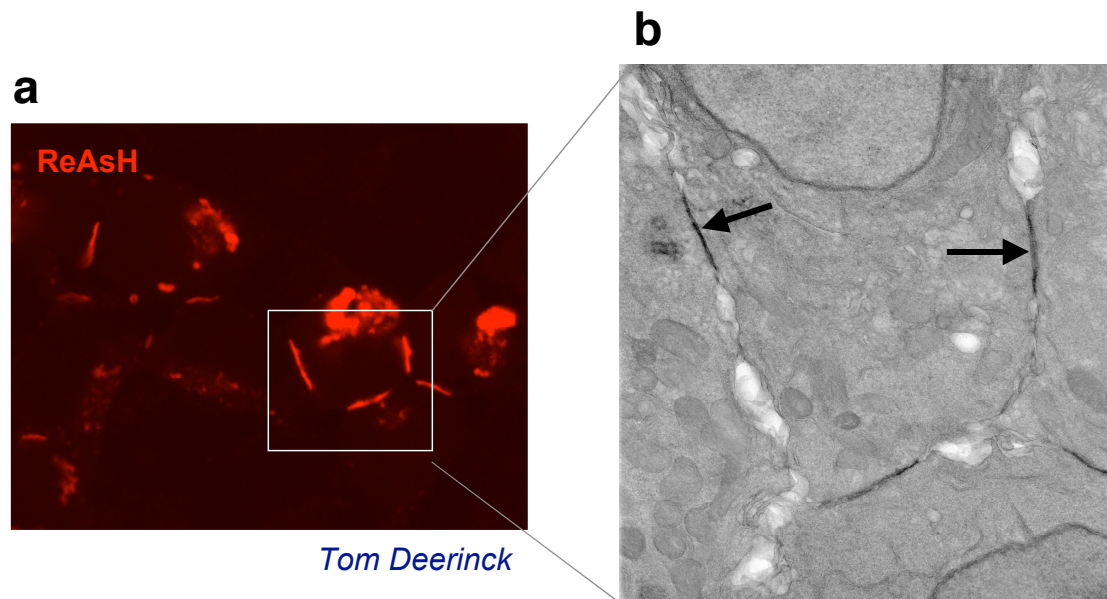


Figure 4.9 Tomography of Cx43-GFP173 (a) ReAsH stained gap junction channels C terminal tagged with GFP173 composite tag. (b) electron micrograph of gap junctions resulting from broadband exposure of ReAsH stained Cx43-GFP173 in the presence of DAP resulting in localized polymerization of the DAP

References

1. Shimomura, O., Johnson, F. H. & Saiga, Y. Extraction, purification and properties of aequorin, a bioluminescent protein from the luminous hydromedusan, *Aequorea*. *J Cell Comp Physiol* **59**, 223-239 (1962).
2. Prasher, D. C., Eckenrode, V. K., Ward, W. W., Prendergast, F. G. & Cormier, M. J. Primary structure of the *Aequorea victoria* green-fluorescent protein. *Gene* **111**, 229-233 (1992).
3. Tsien, R. Y. The green fluorescent protein. *Annu. Rev. Biochem.* **67**, 509-544 (1998).
4. Matz, M. V., Labas, Y. A. & Ugalde, J. Evolution of function and color in GFP-like proteins. *Methods Biochem. Anal.* **47**, 139-161 (2006).
5. Chudakov, D. M., Lukyanov, S. & Lukyanov, K. A. Fluorescent proteins as a toolkit for in vivo imaging. *Trends Biotechnol* **23**, 605-613 (2005).
6. Shaner, N. C., Steinbach, P. A. & Tsien, R. Y. A guide to choosing fluorescent proteins. *Nat Methods* **2**, 905-909 (2005).
7. Cubitt, A. B., Woollenweber, L. A. & Heim, R. Understanding structure-function relationships in the *Aequorea victoria* green fluorescent protein. *Methods Cell Biol.* **58**, 19-30 (1999).
8. Pedelacq, J. D., Cabantous, S., Tran, T., Terwilliger, T. C. & Waldo, G. S. Engineering and characterization of a superfolder green fluorescent protein. *Nat. Biotechnol.* **24**, 79-88 (2006).
9. Bulina, M. E. et al. A genetically encoded photosensitizer. *Nat. Biotechnol.* **24**, 95-99 (2006).
10. Miller, L. W. & Cornish, V. W. Selective chemical labeling of proteins in living cells. *Curr Opin Chem Biol* **9**, 56-61 (2005).
11. Chen, I. & Ting, A. Y. Site-specific labeling of proteins with small molecules in live cells. *Curr. Opin. Biotechnol.* **16**, 35-40 (2005).
12. Gronemeyer, T., Godin, G. & Johnsson, K. Adding value to fusion proteins through covalent labelling. *Curr. Opin. Biotechnol.* **16**, 453-458 (2005).

13. Griffin, B. A., Adams, S. R. & Tsien, R. Y. Specific covalent labeling of recombinant protein molecules inside live cells. *Science* **281**, 269-272 (1998).
14. Adams, S. R. et al. New biarsenical ligands and tetracysteine motifs for protein labeling in vitro and in vivo: synthesis and biological applications. *J. Am. Chem. Soc.* **124**, 6063-6076 (2002).
15. Martin, B. R., Giepmans, B. N., Adams, S. R. & Tsien, R. Y. Mammalian cell-based optimization of the biarsenical-binding tetracysteine motif for improved fluorescence and affinity. *Nat. Biotechnol.* **23**, 1308-1314 (2005).
16. Andresen, M., Schmitz-Salue, R. & Jakobs, S. Short tetracysteine tags to beta-tubulin demonstrate the significance of small labels for live cell imaging. *Mol. Biol. Cell* **15**, 5616-5622 (2004).
17. Hoffmann, C. et al. A FIAsh-based FRET approach to determine G protein-coupled receptor activation in living cells. *Nat Methods* **2**, 171-176 (2005).
18. Dyachok, O., Isakov, Y., Sagetorp, J. & Tengholm, A. Oscillations of cyclic AMP in hormone-stimulated insulin-secreting beta-cells. *Nature* **439**, 349-352 (2006).
19. Enninga, J., Mounier, J., Sansonetti, P. & Tran Van Nhieu, G. Secretion of type III effectors into host cells in real time. *Nat Methods* **2**, 959-965 (2005).
20. Marek, K. W. & Davis, G. W. Transgenically encoded protein photoinactivation (FIAsh-FALI): acute inactivation of synaptotagmin I. *Neuron* **36**, 805-813 (2002).
21. Tour, O., Meijer, R. M., Zacharias, D. A., Adams, S. R. & Tsien, R. Y. Genetically targeted chromophore-assisted light inactivation. *Nat. Biotechnol.* **21**, 1505-1508 (2003).
22. Rice, M. C., Bruner, M., Czymmek, K. & Kmiec, E. B. In vitro and in vivo nucleotide exchange directed by chimeric RNA/DNA oligonucleotides in *Saccharomyces cerevisiae*. *Mol. Microbiol.* **40**, 857-868 (2001).
23. Gaietta, G. et al. Multicolor and electron microscopic imaging of connexin trafficking. *Science* **296**, 503-507 (2002).
24. Ju, W. et al. Activity-dependent regulation of dendritic synthesis and trafficking of AMPA receptors. *Nat Neurosci* **7**, 244-253 (2004).

25. Stroffekova, K., Proenza, C. & Beam, K. G. The protein-labeling reagent FLASH-EDT2 binds not only to CCXXCC motifs but also non-specifically to endogenous cysteine-rich proteins. *Pflugers Arch* **442**, 859-866 (2001).
26. Griffin, B. A., Adams, S. R., Jones, J. & Tsien, R. Y. Fluorescent labeling of recombinant proteins in living cells with FIAsH. *Methods Enzymol.* **327**, 565-578 (2000).
27. Hoebeke, M. & Damoiseau, X. Determination of the singlet oxygen quantum yield of bacteriochlorin a: a comparative study in phosphate buffer and aqueous dispersion of dimiristoyl-L-alpha-phosphatidylcholine liposomes. *Photochem Photobiol Sci* **1**, 283-287 (2002).
28. Beck, S. et al. Fluorophore-assisted light inactivation: a high-throughput tool for direct target validation of proteins. *Proteomics* **2**, 247-255 (2002).
29. Kvam, E., Stokke, T. & Moan, J. The lengths of DNA fragments light-induced in the presence of a photosensitizer localized at the nuclear membrane of human cells. *Biochim. Biophys. Acta* **1049**, 33-37 (1990).
30. Baker, A. & Kanofsky, J. R. Quenching of singlet oxygen by biomolecules from L1210 leukemia cells. *Photochem Photobiol* **55**, 523-528 (1992).
31. Dopf, J. & Horiagon, T. M. Deletion mapping of the *Aequorea victoria* green fluorescent protein. *Gene* **173**, 39-44 (1996).
32. Adzhubei, A. A. & Sternberg, M. J. Left-handed polyproline II helices commonly occur in globular proteins. *J. Mol. Biol.* **229**, 472-493 (1993).
33. Baird, G. S., Zacharias, D. A. & Tsien, R. Y. Circular permutation and receptor insertion within green fluorescent proteins. *Proc Natl Acad Sci U S A* **96**, 11241-11246 (1999).
34. Abedi, M. R., Caponigro, G. & Kamb, A. Green fluorescent protein as a scaffold for intracellular presentation of peptides. *Nucleic Acids Res.* **26**, 623-630 (1998).
35. Giepmans, B. N., Adams, S. R., Ellisman, M. H. & Tsien, R. Y. The fluorescent toolbox for assessing protein location and function. *Science* **312**, 217-224 (2006).

Chapter 5

Genetically Encoded Control of Protein Function

Conclusions

Optical methods to stimulate neurons have proven advantages over classic electrical stimulation methods. Caged optical probes have excellent resolution in space and time, allow parallel stimulation at multiple sites, and are convenient and relatively harmless to cells ^{1,2}. However, photostimulation with caged transmitters has some limitations; action potentials are generated in many neuron types near the stimulation site, the firing timing is not tightly controlled and the caged transmitters are difficult to apply in living animals ¹.

Genetic targeting of neurons allows for selectivity for particular neurons either from specific promoters active in those cells or by using a “gene gun” or viruses to deliver the cDNA in a delimited region remote from the site of eventual illumination. Earlier approaches that use light to depolarize cells and drive neural circuitry ³⁻⁶ have been improved on by using genetically encoded photostimulation through heterologously expressed algal photochannels (CHOP1 and CHOP2)³⁻⁶. Unlike electrical stimulation, glutamate uncaging ⁷ and high-powered laser excitation methods ⁸, ChR2 can be genetically targeted to allow probing of specific neuron subclasses within a heterogeneous neural circuit, avoiding fibers of passage and the simultaneous stimulation of multiple cell types. Functional heterologous expression of the Algal CHOP1 and CHOP2 genes requires supplementation of the cofactor all-

trans retinal as the chromophore⁹. Depending on the cell type targeted for ectopic expression, background levels of retinal were often sufficient to provide a functional chromophore. Most media used for cell culture are sufficient sources of retinal because they contain retinal or its precursor, vitamin A.

The photoactive channel portion of CHOP2 is encoded by a single open reading frame of the first 315 amino acids of the extracted cDNA. A red fluorescent tag mCherry was added to the C terminal of the CHOP2-315 photo-channel to easily identify the cells that were transfected and to verify that there is expression of the channel on the plasmamembrane. As proof of concept, we initially transiently transfected CHOP2-mCherry in mammalian HEK293 cells and then into neurons. The functional expression of the channel was confirmed through electrophysiological whole cell patch clamping of the cell while monitoring the amount of injected current necessary to keep the membrane potential at a clamped voltage of -60mv. Optical calcium reporter techniques were attempted but the action spectrum of the CHOP2-mcherry photo-channel overlapped the FURA2 fluorescent dye calcium reporter excitation wavelength making the logistics complicated for accurate measurements.

Viral vector expression of ChOP2 in specific subpopulations of neurons in the nervous system in transgenic mice should permit the study of the function of individual types of neurons in intact neural circuits and even *in vivo*. Cell-specific promoters will allow targeting of CHOP2 to various well-defined

neuronal subtypes, which will permit future exploration of their causal function in driving downstream neural activity and animal behavior. Understanding precisely which cell types contribute to controlling attention, decision making or action could provide great insight into how they are computed at the circuit level.

The real potential of CHOP2 is in the fast photo-response, both channel activation and deactivation, which can be used to resolve functional connectivity of particular neurons or neuron classes in intact circuits in response to spike trains. Using established electrophysiological current clamping whole cell patch techniques, measurements have been made characterizing the neuronal pulse train response of hippocampal neurons¹⁰

The light power required for ChR2 activation ($8\text{-}12\text{ mW/mm}^2$) is fairly low. For CHOP2 to be an effective tool for *in vivo* studies of circuit maps and behavior, light stimulus delivery via optic fiber is an effective albeit invasive method of delivery. An inherent problem with superficial light stimulation is that the tissue penetration depth is very shallow due to scattering. Tissue scattering and absorption decreases steeply as wavelengths increase.

Red shifting the activation spectrum of the CHOP channels might be approached by either changing the retinal chromophore or by changing the amino acid environment of the all trans retinal binding pocket or both. Changes to amino acids surrounding the all trans retinal chromophore have been extensively characterized with respect to the binding pocket of

bacteriorhodopsin. In order for the bacterium to engage in photosynthesis with reasonable efficiency, the absorbance spectrum of the chromophore has to overlap with the solar irradiance, which is peaked near 500 nm. When linked to an unprotonated Schiff base in methanol solution, *all-trans* retinal has an absorbance maximum near 360 nm¹¹. When the Schiff base is protonated, the absorbance shifts to about 450 nm¹¹. When bound to bR through a protonated Schiff base linkage, the absorbance is further shifted to about 570 nm. This “opsin” shift¹² optimizes the retinal absorbance for carrying out photosynthesis. Through directed mutagenesis of the residues influencing the retinal binding pocket, the opsin shift can be further extended to longer wavelengths. The maximum action spectrum red shift so far achieved by mutating the bR retinal binding pocket is on the order of 120nm. A similar shift of the CHOP2 action spectrum would give a 600nm peak.

A more promising approach might be to substitute the retinal chromophore with a retinal analog that red shifts the action spectrum of the heterologously chlamydomonas opsin. Azulenic retinals had been successfully incorporated into a retinal-deficient strain of *Chlamydomonas* with restoration of phototactic response to near IR-light¹³, with a fitted peak at 674nm (K.W. Foster, personal communication). If the heterologously expressed chlamy-opsin photo-channel could be activated by IR or near-IR wavelengths instead of 480-500 nm, its usefulness in complex neural tissues would be much enhanced. Unfortunately it is not known which *Chlamydomonas* opsin mediated the far-red response. Further experiments are necessary to

determine if the retinal analog works with the CHOP2 ion photo-channel expressed heterologously.

The CHOP2 photo-channel is capable of inducing photo-modulated neuronal responses achieving the aim for noninvasive, genetically targeted, temporally precise control of neuronal activity, with potential applications ranging from neuroscience to biomedical engineering. One in-vivo application that exemplifies the efficacy of the CHOP2 channel is been demonstrated in restoring the light sensitivity to photoreceptor cells¹⁴.

In the retina, photoreceptor cells convert light signals to electrical signals that are then relayed through second- and third-order retinal neurons to higher visual centers in the brain^{15,16}. The severe loss of photoreceptor cells caused by congenital retinal degenerative diseases, such as retinitis pigmentosa (RP)¹⁷⁻¹⁹, often results in complete blindness. Previous studies reported the heterologous expression of *Drosophila* rhodopsin⁶ and, more recently, melanopsin, the putative photopigment of the intrinsic photosensitive retinal ganglion cell²⁰⁻²². These photopigments, however, are coupled to membrane channels via a G protein signaling cascade and use -isoforms of retinaldehyde as their chromophore. As a result, expression of multiple genes would be required to render photosensitivity. In addition, their light response kinetics is rather slow.

Multi ReAsH fluorophore reporters in living organisms

One of the most dramatic applications of GFP-protein fusions has been noninvasive imaging of protein expression and localization in living organisms

ranging from bacteria and *Caenorhabditis elegans* to mice. Biarsenical chemical reporters can likewise tag recombinant proteins. The biarsenical-tetracysteine pair has often been scrutinized in comparison with fluorescent proteins. Here we have considered the fluorescent protein GFP rigid structure as a scaffold to multimerize biarsenical-tetracysteine motifs.

Placing additional fluorophores on the GFP scaffold would be constructive and contribute to decreasing the detection limits of biarsenical dyes. In carefully constructing multiple chromophore arrangements on GFP, we have been able to avoid fluorescence quenching. We have demonstrated a general relationship between the fluorescent quantum yield and the singlet oxygen quantum yield though the multiple chromophore response to generating singlet oxygen is less predictable.

The TC-GFP composite construct with an optimized tetracysteine on the N terminal and inserted before residue 173 of GFP (C4GFP173C4) is the construct with the highest double TC singlet oxygen quantum yield (0.036) while retaining a reasonable fluorescent quantum yield (0.33). The gap junction protein, Connexin43, has been shown in the laboratory to tolerate a C terminal optimized TC with out compromising the biarsenical binding or gap junction function. Dr. Thomas Deerinck observed that the double TC-GFP tag has a ReAsH:GFP ratio that is 2.5 times greater than the single TC-GFP composite tag ReAsH:GFP ratio on Cx43. The ratio of the in-vitro measured fluorescent quantum yields (1.43) of the two TC to the one TC composite tags is much lower than the ratio of the relative ReAsH fluorescent brightness of the two TC to the one TC composite

tag on Cx43 in cells. In the case of Cx43, the protein fusion seems to be beneficial to the overall function of the C4GFP173X4 tag. It is not surprising that the N terminal TC is impacted by the fusion to the Cx43. It was the original intent the composite tag would function autonomously.

The construct with an optimized tetracysteines inserted before residues 173 and 192 has a singlet oxygen and fluorescent quantum yields that are the average of the individual quantum yields. The GFP fluorescence is somewhat compromised but it has utility in that neither of the TCs are influenced by the fusion to a protein of interest.

References

1. Callaway, E. M. & Yuste, R. Stimulating neurons with light. *Curr. Opin. Neurobiol.* **12**, 587-592 (2002).
2. Miesenbock, G. Genetic methods for illuminating the function of neural circuits. *Curr. Opin. Neurobiol.* **14**, 395-402 (2004).
3. Lima, S. Q. & Miesenbock, G. Remote control of behavior through genetically targeted photostimulation of neurons. *Cell* **121**, 141-152 (2005).
4. Banghart, M., Borges, K., Isacoff, E., Trauner, D. & Kramer, R. H. Light-activated ion channels for remote control of neuronal firing. *Nat Neurosci* **7**, 1381-1386 (2004).
5. Zemelman, B. V., Nesnas, N., Lee, G. A. & Miesenbock, G. Photochemical gating of heterologous ion channels: remote control over genetically designated populations of neurons. *Proc Natl Acad Sci U S A* **100**, 1352-1357 (2003).
6. Zemelman, B. V., Lee, G. A., Ng, M. & Miesenbock, G. Selective photostimulation of genetically chARGed neurons. *Neuron* **33**, 15-22 (2002).
7. Dantzker, J. L. & Callaway, E. M. Laminar sources of synaptic input to cortical inhibitory interneurons and pyramidal neurons. *Nat Neurosci* **3**, 701-707 (2000).
8. Hirase, H., Nikolenko, V., Goldberg, J. H. & Yuste, R. Multiphoton stimulation of neurons. *J. Neurobiol.* **51**, 237-247 (2002).
9. Nagel, G. et al. Channelrhodopsin-1: a light-gated proton channel in green algae. *Science* **296**, 2395-2398 (2002).
10. Boyden, E. S., Zhang, F., Bamberg, E., Nagel, G. & Deisseroth, K. Millisecond-timescale, genetically targeted optical control of neural activity. *Nat Neurosci* **8**, 1263-1268 (2005).
11. Koyama, Y., Kubo, K., Komori, M., Yasuda, H. & Mukai, Y. Effect of protonation on the isomerization properties of n-butylamine Schiff base of isomeric retinal as revealed by direct HPLC analyses: selection of isomerization pathways by retinal proteins. *Photochem Photobiol* **54**, 433-443 (1991).

12. MG, M. et al. Electron Transfer: Classical Approaches and New Frontiers. *Journal American Chemical Society* **102**, 7947 (1980).
13. Asato, A. E., Peng, A., Hossain, M. Z., Mirzadegan, T. & Bertram, J. S. Azulenetic retinoids: novel nonbenzenoid aromatic retinoids with anticancer activity. *J. Med. Chem.* **36**, 3137-3147 (1993).
14. Bi, A. et al. Ectopic expression of a microbial-type rhodopsin restores visual responses in mice with photoreceptor degeneration. *Neuron* **50**, 23-33 (2006).
15. Baylor, D. How photons start vision. *Proc Natl Acad Sci U S A* **93**, 560-565 (1996).
16. Kalloniatis, M., Sun, D., Foster, L., Haverkamp, S. & Wassle, H. Localization of NMDA receptor subunits and mapping NMDA drive within the mammalian retina. *Vis Neurosci* **21**, 587-597 (2004).
17. Sung, C. H., Schneider, B. G., Agarwal, N., Papermaster, D. S. & Nathans, J. Functional heterogeneity of mutant rhodopsins responsible for autosomal dominant retinitis pigmentosa. *Proc Natl Acad Sci U S A* **88**, 8840-8844 (1991).
18. Humphries, P., Kenna, P. & Farrar, G. J. On the molecular genetics of retinitis pigmentosa. *Science* **256**, 804-808 (1992).
19. Fishman, G. A. et al. Effect of methazolamide on chronic macular edema in patients with retinitis pigmentosa. *Ophthalmology* **101**, 687-693 (1994).
20. Melyan, Z., Tarttelin, E. E., Bellingham, J., Lucas, R. J. & Hankins, M. W. Addition of human melanopsin renders mammalian cells photoresponsive. *Nature* **433**, 741-745 (2005).
21. Panda, S. et al. Illumination of the melanopsin signaling pathway. *Science* **307**, 600-604 (2005).
22. Qiu, X. et al. Induction of photosensitivity by heterologous expression of melanopsin. *Nature* **433**, 745-749 (2005).